Article

Optimized Bentonite Clay Adsorbents for Methylene Blue Removal

Hamad Noori Hamad [1], Syazwani Idrus [1,*], Badronnisa Yusuf [1], Nur Syakina Jamali [2], Amimul Ahsan [3,4], Sri Suhartini [5] and Abdul Malek Abdul Wahab [6]

1   Department of Civil Engineering, Faculty of Engineering, Universiti Putra Malaysia, Serdang 43400, Malaysia; gs59432@student.upm.edu.my (H.N.H.); nisa@upm.edu.my (B.Y.)
2   Department of Chemical and Environmental Engineering, Faculty of Engineering, Universiti Putra Malaysia, Serdang 43400, Malaysia; syakina@upm.edu.my
3   Department of Civil and Environmental Engineering, Islamic University of Technology (IUT), Gazipur 1704, Bangladesh; aa@iut-dhaka.edu
4   Department of Civil and Construction Engineering, Swinburne University of Technology, Melbourne 3122, Australia
5   Department of Agro-industrial Technology, Faculty of Agricultural Technology, Universitas Brawijaya, Malang 65145, Indonesia; ssuhartini@ub.ac.id
6   School of Mechanical Engineering, College of Engineering, Universiti Teknologi MARA, Shah Alam 40450, Malaysia; abdmalek@uitm.edu.my
*   Correspondence: syazwani@upm.edu.my; Tel.: +60-13-692-2301

Abstract: This study addresses the urgent need for effective water treatment methods by synthesizing and characterizing activated bentonite clay (ABC) adsorbents to remove methylene blue (MB) from aqueous solutions efficiently. Conventional adsorbents often exhibit limitations in efficiency and regeneration capabilities, necessitating novel approaches to water treatment. The primary objective is synthesizing and characterizing high-quality ABC adsorbents capable of effectively removing MB. The activation process was optimized, and adsorbent performance was evaluated regarding MB removal efficiency and regeneration potential. Various activation dos-ages were investigated, and comprehensive physicochemical characterization was performed using scanning electron microscopy (SEM), Fourier transform infrared spectroscopy (FTIR), BET (Brunauer–Emmett–Teller) analysis, X-ray fluorescence (XRF), thermogravimetric analysis (TGA), and X-ray diffraction (XRD). The synthesized adsorbents demonstrated exceptional MB removal efficiency (99.593%) and impressive adsorption capacity (22.131 mg/g) when activated with 16 M sodium hydroxide. The adsorption process exhibited spontaneity and exothermicity, as validated by Freundlich and second-order kinetic models. Furthermore, the adsorbents showcased successful regeneration and reusability over three cycles, highlighting their potential for long-term application in water treatment. This study significantly advances water treatment by offering a novel approach to MB removal using base-activated bentonite clay (BABC) adsorbents, contributing to the development of sustainable water treatment solutions.

Keywords: methylene blue removal; bentonite clay; adsorption; isotherm; low-cost adsorbents; drinking water; cationic dyes

1. Introduction

Synthetic dyes, especially methylene blue (MB), pose a formidable challenge to environmental sustainability, significantly contributing to water pollution [1]. With the capacity to be detected in water at minimal concentrations (as low as one mg/L) and commonly found in textile effluents at levels ranging from 10 to 200 mg/L [2], the prevalence of MB across diverse industrial applications, including textiles, printing, and cosmetics, has led to its widespread dissemination into aquatic environments [3,4]. This threatens ecosystem integrity and poses substantial risks to human health [5], necessitating urgent and effective

solutions for MB decontamination to ensure the safety of drinking water supplies and mitigate adverse environmental impacts [6].

To address this pressing concern, recent research efforts have increasingly concentrated on developing effective and sustainable methodologies for MB remediation from aqueous solutions [7]. Among these, adsorption emerges as an up-and-coming technique attributed to its efficiency, versatility, and potential for utilizing a wide array of modified materials as adsorbents [8]. This approach seeks to surpass the limitations inherent to conventional adsorbents, driving the exploration of novel materials characterized by enhanced MB removal capabilities [9,10].

Bentonite clay (BC), recognized for its abundant availability, cost-effectiveness, and remarkable adsorption capacity, has attracted considerable attention as a potential adsorbent for dye remediation [11,12]. Previous studies have highlighted the effectiveness of BC in adsorption and separation, emphasizing its high cation exchange capacity, stability, and strong adsorption capabilities [13,14]. Nonetheless, the realization of BC's full adsorptive potential typically necessitates chemical modifications aimed at augmenting its surface area and the availability of adsorption sites, thereby significantly boosting its performance in dye removal applications [15].

While existing literature predominantly focuses on the activation of BC using high concentrations of sulfuric acid (H_2SO_4) [16–19] and hydrochloric acid (HCl) [20,21], processes that have been shown to enhance the clay's surface area and porosity. The exploration of sodium hydroxide (NaOH) activation through the reflux method for MB removal represents a relatively uncharted research avenue. This novel approach harbors the potential to enhance the adsorption properties and surface reactivity of BC and develop mesoporous structures conducive to improved adsorptive efficiency. Furthermore, NaOH is positioned as an environmentally friendlier alternative to other chemical activators, such as KOH, owing to its reduced corrosivity and associated hazards [22–24].

Regarding the sustainability concerns raised, although NaOH activation involves both a base (NaOH) solution and heating, the process remains relatively sustainable when considering the benefits of reduced waste generation and enhanced adsorption capacity [25]. Compared to alternative methods, NaOH activation offers several advantages, such as lower costs and fewer hazards, contributing to its sustainability [22,23].

Emerging research highlights the efficacy of NaOH activation in bolstering adsorbent capacity and advancing sustainable practices within wastewater treatment. These findings underscore NaOH activation's potential in augmenting adsorption capacity for MB removal [26–29].

This research endeavor seeks to pioneer the investigation into the NaOH activation of BC for MB removal to bridge these existing knowledge gaps by investigating these innovative activation techniques, employing an array of sophisticated characterization techniques—including X-ray fluorescence (XRF) analysis, scanning electron microscopy (SEM), Fourier transform infrared spectroscopy (FTIR), Brunauer–Emmett–Teller (BET) analysis, thermogravimetric analysis (TGA), and X-ray diffraction (XRD). This study is poised to significantly contribute to advancing adsorption science and environmental engineering through a meticulous evaluation encompassing MB removal efficiency, optimization protocols, isotherm and kinetic modeling, thermodynamic insights, and regeneration and reusability assessments. By elucidating efficient and environmentally benign methodologies for MB remediation, this investigation aims to expand the scientific understanding of adsorbent materials and foster the development of sustainable water treatment solutions.

As such, the narrative arc of this paper unfolds across three principal sections, commencing with an elucidation of materials and methods, advancing through a comprehensive discussion of results, and culminating in a conclusion that encapsulates the study's key findings and implications for future research.

2. Materials and Methods

2.1. Materials

For the experimental investigations, the target pollutant was MB powder with a chemical formula of $C_{16}H_{18}N_3SCl$ and 319.85 g/mol of molecular weight obtained from Chemiz Malaysia Sdn Bhd. Pure BC purchased from R&M Chemicals Malaysia Sdn Bhd (Semenyih, Malaysia) was used as the adsorbent to remove MB from aqueous solutions.

2.2. Activation of Bentonite Clay Methods

The synthesis of activated bentonite clay (ABC) involved two distinct activation methods, utilizing sulfuric acid (H_2SO_4 98%) and sodium hydroxide (NaOH). The activation process incorporated slight modifications based on previous studies [13,30,31]. The BC was initially washed with distilled water to eliminate impurities, followed by drying in an oven at 100 °C and subsequent fine grinding. Figure 1 illustrates the comprehensive flowchart outlining the process of preparing ABC.
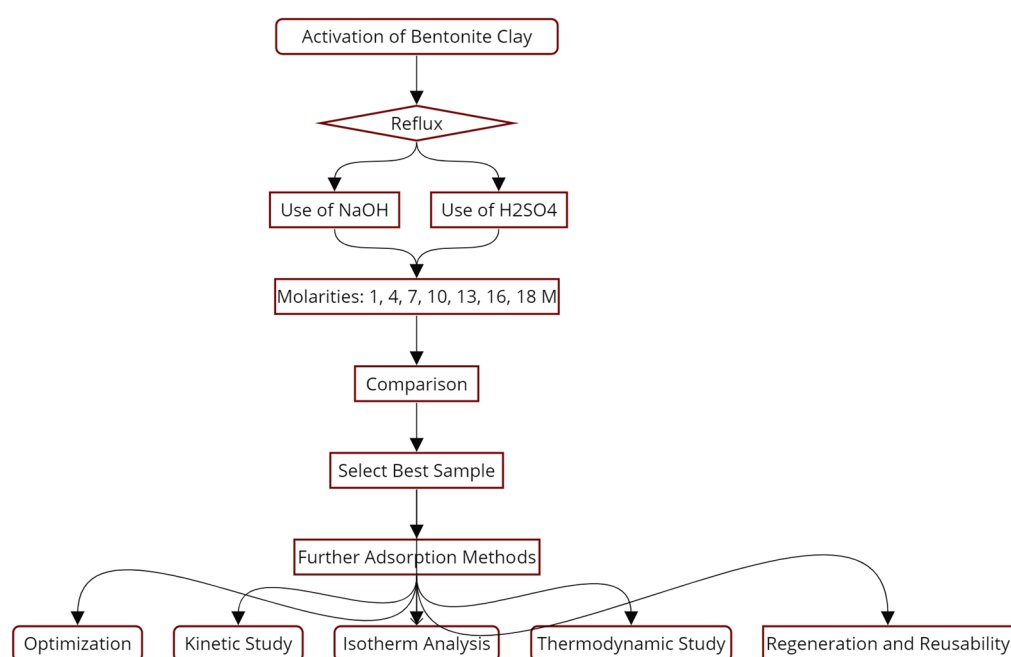
Figure 1. Diagram of the process flow of activated bentonite clay's preparation.

In the acid-activated bentonite clay (AABC) procedure, chemically pure BC was combined with varying concentrations of sulfuric acid (H_2SO_4 98%) (1 M, 4 M, 7 M, 10 M, 13 M, 16 M, and 18 M). The mixture underwent reflux at 110 °C and 35 rpm for 3 h, with a ratio of 8 g of BC to 70 mL of sulfuric acid solution. Following reflux, the activated clay was washed until reaching a pH of 7, then dried at 100 °C for 3 h, ground, and stored.

Similarly, for base-activated bentonite clay (BABC), washed BC was mixed with different sodium hydroxide concentrations (1 M, 4 M, 7 M, 10 M, 13 M, 16 M, and 18 M). The mixture underwent reflux at 110 °C and 35 rpm for 3 h, with a ratio of 8 g of BC to 70 mL of sodium hydroxide solution. The base-activated clay was washed until reaching a pH of 7, followed by drying at 100 °C for 3 h, grinding, and storage. Figure 2 displays samples of both AABC and BABC post-activation.

Figure 2. All samples of acid-activated bentonite clay (AABC) and base-activated bentonite clay (BABC).

2.3. Surface Characterization

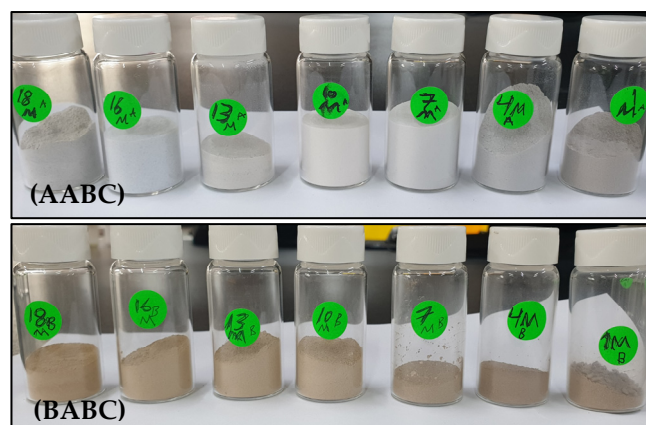The surface characterization of the ABC was conducted using various analytical techniques. Thermogravimetric analysis (TGA) was performed with a METTLER TOLEDO TGA/DSC3+ instrument (Greifensee, Switzerland) to assess the raw BC's thermal stability and decomposition behavior. X-ray fluorescence (XRF) analysis, conducted with an EDX-720 SHIMADZU instrument (Kyoto, Japan), determined the elemental composition of the ABC, providing insights into the types and quantities of elements present. The ABC's specific surface area and pore size distribution were evaluated through Brunauer–Emmett–Teller (BET) analysis, performed with a MICROMERITICS 3FLEX instrument (Norcross, GA, USA) at a degassing temperature of N_2 (77 K). Scanning Electron Microscopy (SEM) using an S3400-N HITACHI instrument (Tokyo, Japan) allowed for the examination of the surface morphology and microstructure of the ABC, providing high-resolution images for observing surface features and particle size. Fourier transform infrared spectroscopy (FTIR), conducted with a SPECTRUM 100 PERKIN ELMER instrument (Waltham, MA, USA) in the spectrum range of 650–4000 cm^{-1}, identified the functional groups in the ABC, aiding in the characterization of chemical bonds and molecular structure. Lastly, X-ray diffraction (XRD) analysis, performed with XRD6000 SHIMADZUI equipment (Kyoto, Japan) at a 2-theta degree (2θ)-diffraction angle, investigated the crystalline structure and phase composition of the ABC, offering information about the atomic arrangement and the presence of specific crystalline phases.

2.4. Batch Experimentation

In this section, optimization studies were conducted for batch experimentation to improve ABC adsorption capacity (*q*) for the removal of MB. Various parameters, such as contact time (0–315 min), initial concentration (50–200 ppm), temperature (25–50 °C), pH (4–10), and dosage (0.5–0.95 g), were systematically investigated to assess their impact on adsorption efficiency. The adsorption capacity (*q*), a critical metric quantifying the maximum adsorbate binding per unit mass or volume on the adsorbent, was determined using the formula presented in Equation (1) [32–34]:

$$q = \frac{(Ci - Ce)}{v} \times m \tag{1}$$

The variables in the formula represent the following: *q* is the adsorption capacity, C_i is the initial adsorbate concentration, C_e is the equilibrium adsorbate concentration, *v* is the solution volume, and *m* is the adsorbent mass.

Various isotherm models, including Langmuir, Freundlich, Temkin, and Dubinin–Radushkevich (D–R), were utilized to explore the relationship between adsorbate concentration in the solution and its interaction with the adsorbent material [32–34]. The Langmuir model, representing monolayer adsorption on a uniform surface, is defined

by Equation (2). The Freundlich model, accommodating heterogeneous adsorption, is articulated in Equation (3). The Temkin model, which considers interactions between adsorbent and adsorbate, is expressed in Equation (4). The Dubinin–Radushkevich model, describing adsorption on heterogeneous surfaces, is formulated in Equation (5). Kinetic adsorption studies employing the pseudo-first-order (Equation (6)) and pseudo-second-order (Equation (7)) models were conducted to elucidate the adsorption rate over time [33–35]. Thermodynamic analysis, vital for understanding the spontaneity, randomness, and energetics of the adsorption process, involves parameters such as Gibbs free energy (ΔG), calculated using Equation (8) [33–35]. Enthalpy (ΔH) and entropy (ΔS), revealing the energy and randomness of adsorption, are determined using the van't Hoff equation in Equation (9) [34,36]:

$$q = \frac{Qm \times b \times c}{1 + b \times c} \tag{2}$$

$$q = KF \times C^{\frac{1}{n}} \tag{3}$$

$$q = \frac{RT}{bT} \times \ln(A \times C) \tag{4}$$

$$q = qo \times \exp\left(-\beta \times \varepsilon^2\right) \tag{5}$$

$$\log(qe - qt) = \log(qe) - \frac{K1}{2.303} \times t \tag{6}$$

$$\frac{t}{qt} = \frac{1}{K2 \times qe^2} + \frac{t}{qe} \tag{7}$$

$$\Delta G = -RT\ln(K) \tag{8}$$

$$\ln(K) = -\frac{\Delta H}{R} + \frac{\Delta S}{R} \times \frac{1}{T} \tag{9}$$

where Q_m (mg/g): maximum adsorption capacity; b (L/mg): Langmuir constant; C (mg/L): equilibrium concentration of the adsorbate; K_F (mg/g) (L/mg)$^{(1/n)}$: Freundlich constant; n: Freundlich exponent; b_T (J/mol): Temkin constant; A (L/g): Temkin isotherm constant; q_o (mg/g): maximum adsorption capacity in the D–R model; β (mol^2/kJ^2): D–R constant; ε (kJ/mol): Polanyi potential; k_1 (1/min), k_2 (g/mg min): rate constants in kinetic models; ΔG (kJ/mol): Gibbs free energy; ΔH (kJ/mol): enthalpy change; ΔS (kJ/mol): entropy change; R (J/mol K): gas constant (8.314); T: temperature in Kelvin; and K (dimensionless): equilibrium constant.

2.5. Regeneration and Reusability

The regeneration study of ABC employed four techniques. The spent adsorbents were stirred using equipment (digital heating mantle with stirring (DMS series (MTOPS)) with sodium persulfate ($Na_2S_2O_8$) (1:2) at 80 °C and 15 rpm for 1 and 2 h using different volumes: 70 mL for 1 h, 70 mL for 2 h, 250 mL for 1 h, and 250 mL for 2 h.

After each cycle, the adsorbents' reusability was assessed by subjecting them to multiple adsorption cycles under the same optimized conditions. The regeneration and reusability efficiency were evaluated based on the percentage of the initial adsorption capacity of the fresh adsorbents.

3. Results and Discussion

3.1. Surface Characterization of ABC

3.1.1. TGA Analysis

Thermogravimetric analysis (TGA) was performed on the raw BC sample to assess its thermal stability and composition. The investigation extensively explored the thermal behavior of the clay across a temperature range of 25–150 °C, as depicted in Figure 3.
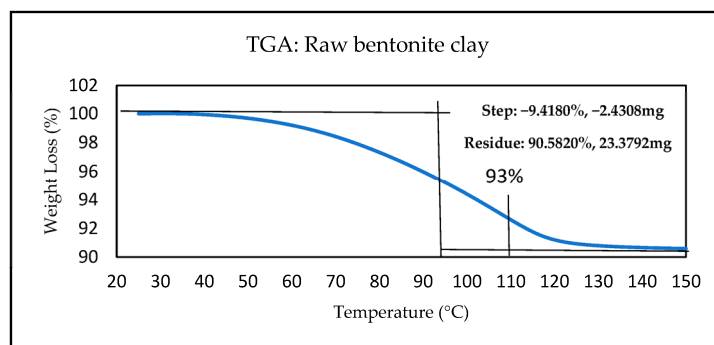
Figure 3. TGA: raw bentonite clay.

The thermal behavior of untreated BC was investigated using TGA analysis over a temperature range of 25–150 °C. The study was carried out with precise weight loss monitoring using steps of −9.4180% and −2.4308 mg. Initial stages indicated a weight loss of −9.4180%, attributed to removing volatile components. Despite this, a significant residue of 90.5820% (23.3792 mg) remained, indicating the overall composition of the clay remained unchanged. Similar observations were reported in studies by [37,38]. Remarkably, the clay exhibited notable stability at 110 °C with a residue of approximately 93%, confirming the retention of its essential adsorption capabilities. These findings align with previous research, including about 93% by [37], about 96% by [38], and around 94.5% by [39]. This approach effectively balances temperature control while preserving critical clay layers, including silica and alumina.

3.1.2. XRF Analysis

The XRF analysis delineated notable compositional transformations between the raw BC and the optimal activation dosages of AABC and BABC, as tabulated in Table 1. Initially, the raw clay displayed a SiO_2 content of 52.39%, with corresponding Al_2O_3, Na_2O, and MgO contents of 18.69%, 2.147%, and 2.357%, respectively. Upon acid activation (AABC), the SiO_2 content surged to 79.121%, accompanied by diminished levels of Al_2O_3, Na_2O, and MgO. Conversely, base activation (BABC) reduced SiO_2 content to 47.353%, coupled with a substantial increase in Al_2O_3, Na_2O, and MgO contents (31.294, 12.001, and 3.182, respectively). Other trace elements exhibited relatively minor fluctuations in concentration. These alterations bear significant implications for the adsorption characteristics of the activated clays.

Table 1. XRF chemical compositions of raw and activated bentonite clay (16 M BABC, 7 M AABC).

Compound	Raw BC %	BABC (16 M) %	AABC (7 M) %
SiO_2	52.390	47.353	79.121
Al_2O_3	18.690	31.294	11.920
Na_2O	2.147	12.001	0.089
MgO	2.357	3.182	0.644
MnO	0.526	0.568	0.013
ZnO	0.080	0.095	0.014
K_2O	0.278	0.183	0.121
CaO	0.968	1.732	0.342
TiO_2	1.291	1.471	2.245

The augmentation of SiO_2 content in AABC signifies an enriched adsorption potential, whereas the heightened Al_2O_3 content in BABC implies enhanced adsorption properties. Moreover, the elevated Na_2O content in BABC fosters ion exchange mechanisms, positively impacting the adsorption of cationic dyes like MB. The consistent MgO content across both activated clays suggests its marginal involvement in the activation process. Notably, BABC showcases the most promising composition for efficient MB adsorption, owing to

its elevated SiO_2, Al_2O_3, MgO, and Na_2O content. This positions BABC as a preferential candidate for water treatment applications [17,37].

3.1.3. BET Analysis

BET analysis was conducted on raw and base-activated bentonite clay (BABC) specimens across a spectrum of NaOH activation dosages (1 M to 18 M) alongside an acid-activated bentonite clay (AABC) sample at an optimal dosage of 7 M to evaluate surface area, pore volume, and pore size under nitrogen degassing at 77 K. These parameters, indicative of the material's porosity and potential as an adsorbent, are summarized in Table 2 for raw BC and activated samples.

Table 2. BET: surface area and porosity characteristics of raw BC, BABC, and the optimal AABC sample.

	BC	BABC							AABC
Activation	**Raw**	**1 M**	**4 M**	**7 M**	**10 M**	**13 M**	**16 M**	**18 M**	**7 M**
Surface Area (m^2/g)	8.86	30.90	55.71	70.72	65.20	60.28	74.15	51.97	42.76
Pore Volume (cm^3/g)	0.22	0.38	0.72	1.01	0.73	0.80	1.11	0.69	0.106
Pore Size (Å)	162.4	246.01	259.23	288.37	225.69	266.75	300.20	266.78	121.23

Raw BC demonstrated initial porosity characteristics with a surface area of 8.86 m^2/g, a pore volume of 0.22 cm^3/g, and a pore size of 162.6 Å (16.26 nm), categorizing it within the mesoporous range [40]. An increase in NaOH concentration from 1 M to 4 M enhanced the surface area to 55.71 m^2/g and the pore volume to 0.72 cm^3/g, with a corresponding pore size increase to 259.23 Å (25.923 nm), further confirming the mesoporous nature of the samples and indicating enhanced porosity.

At a NaOH dosage of 7 M, a notable peak in surface area (70.72 m^2/g) and pore volume (1.01 cm^3/g) was observed, along with a pore size of 288.37 Å (28.837 nm), suggesting an optimal enhancement of mesoporosity. This suggests an effective porosity augmentation, likely due to the optimal disruption of the clay matrix and the formation of new pores. However, subsequent increases in NaOH dosage to 10 M and 13 M resulted in slight reductions in surface area and pore volume, with pore sizes of 225.69 Å (22.569 nm) to 266.75 Å (26.675 nm). This decline may be attributed to the aggregation of particles or the enlargement of existing pores beyond the optimal mesoporous range, potentially hindering the material's adsorption efficiency due to excessive NaOH concentration.

Contrastingly, at 16 M NaOH, the surface area was resurgent (74.15 m^2/g) and the pore volume was 1.11 cm^3/g, with the pore size expanding to 300.20 Å (30.020 nm), indicating the presence of larger mesopores. This suggests that the conditions at this concentration are conducive to maximizing porosity without compromising the integrity of the pore structure, thus enhancing the clay's adsorption potential.

Interestingly, even at an 18 M NaOH dosage, while the surface area decreased to 51.97 m^2/g, it remained above that of the untreated clay, highlighting the effectiveness of NaOH activation in improving porosity, albeit with a reduced pore volume and size (0.106 cm^3/g, 121.23 Å, or 12.123 nm), suggesting a shift towards smaller mesopores or potentially micropores.

Compared to the optimal 7 M AABC activation, which yielded a surface area of 42.76 m^2/g and a pore volume of 0.106 cm^3/g with a pore size of 121.23 Å (12.123 nm), the 16 M BABC activation displayed a superior surface area and pore volume [37]. This positions BABC, particularly at the 16 M dosage, as a more effective adsorbent for methylene blue (MB) removal, demonstrating significant potential for environmental applications. The observed trends in surface area, pore volume, and pore size across different activation dosages underscore the nuanced impact of NaOH activation on the material's porosity and its implications for adsorption efficiency [37,40–43].

3.1.4. SEM Analysis

Surface morphology and microstructural features of BC samples subjected to distinct activation methods were investigated via SEM analysis. A comparative study was conducted between acid activation with H_2SO_4 (AABC) and base activation with NaOH (BABC), revealing pronounced distinctions through SEM analysis. Images of AABC (7 M) and BABC (16 M) samples exhibited apparent variations in surface morphology. In contrast, the BABC showcased a refined, well-defined structure with enhanced particle connectivity and uniformity. Particle aggregation was also examined, highlighting reduced accumulation in the BABC, signifying better dispersion and heightened accessibility to active sites, akin to findings from earlier studies on acid-activated clay [17,44].

Furthermore, SEM analysis unveiled insights into pore structures, with base activation yielding more open and evenly distributed pores, amplifying the clay's adsorption capacity and reactivity. The SEM images indicated a more uniform particle size and shape distribution in the BABC, indicative of a controlled and optimized activation process. The BABC demonstrated heightened homogeneity due to the specific interaction between NaOH and the clay structure. Figure 4 presents the SEM characterization analysis of the optimal activation samples, including raw (a)–(d), AABC (e)–(h), and BABC (i)–(l) (at varying scales (200 μm; 50 μm; 10 μm; 3 μm, respectively).
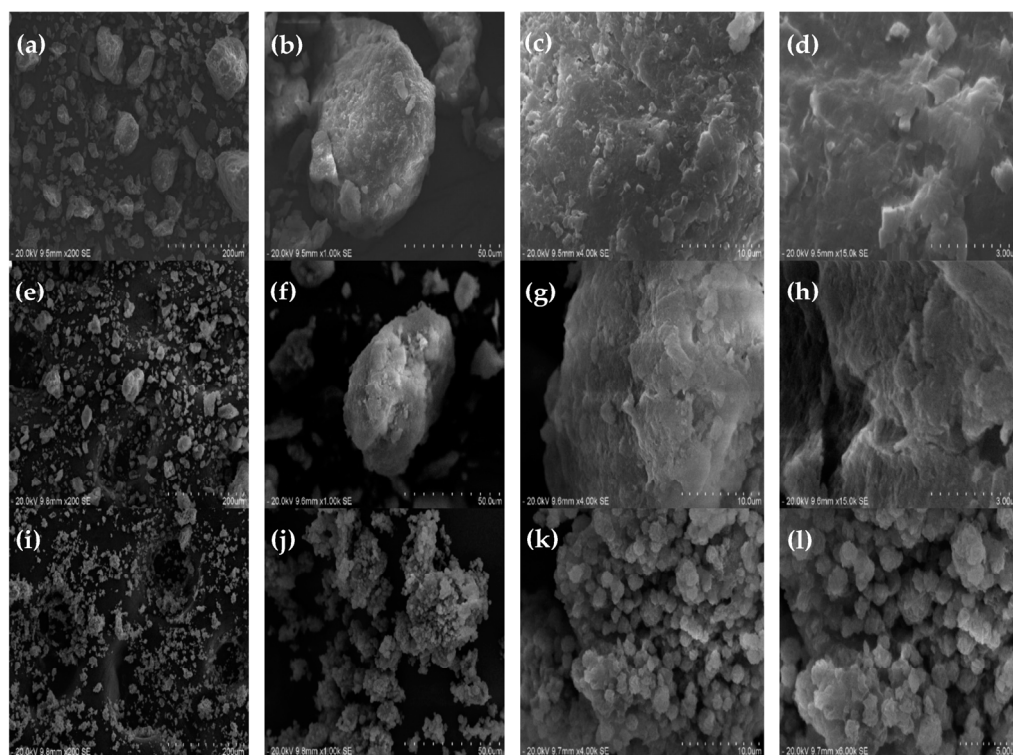

Figure 4. SEM images depicting the effect of activation dosage on the morphology of BC. (**a**–**d**): corresponding to raw BC; (**e**–**h**): corresponding to 7 M of AABC; (**i**–**l**): corresponding to 16 M of BABC at varying scales (200 μm; 50 μm; 10 μm; 3 μm, respectively).

3.1.5. FTIR Analysis

FTIR analysis (650–4000 nm) was conducted on BABC samples activated with various dosages of (1 M, 4 M, 7 M, 10 M, 13 M, 16 M, and 18 M) shown in Figures 5 and 6, and AABC of the optimal activation dosage of (7 M) presented in Figure 7, to investigate changes in functional groups and assess the impact of activation dosage. The raw clay exhibited peaks at 3623.71 cm^{-1}, 3408.81 cm^{-1}, and 2324.67 cm^{-1}, indicating the presence of hydroxyl groups, water molecules, and adsorbed CO_2. Peaks at 1738.71 cm^{-1}, 1638.06 cm^{-1}, and 1472.56 cm^{-1} suggested the presence of carbonyl groups and organic compounds, while peaks at 1009.97 cm^{-1}, 917.12 cm^{-1} and 789.89 cm^{-1} indicated the presence of Si-O bonds,

Si-O-Si bonds, and Si-O-Al bonds, respectively. The peak at 692.84 cm^{-1} suggested the presence of Si-O-Mg bonds. Activation with (NaOH) BABC resulted in variations in the peaks associated with hydroxyl groups, water molecules, carbonyl groups, Si-O stretching vibrations, and bending vibrations of Al-OH groups [45–47]. Activation with (H$_2$SO$_4$) AABC showed peaks related to hydroxyl groups, water molecules, carbonyl groups, Si-O bending and stretching vibrations, as well as stretching vibrations of Si-O bonds and Si-O-Si bonds [17,46]. Figures 5 and 6 illustrate the FTIR characterization analysis of raw BC and BABC activated by (1–18 M).
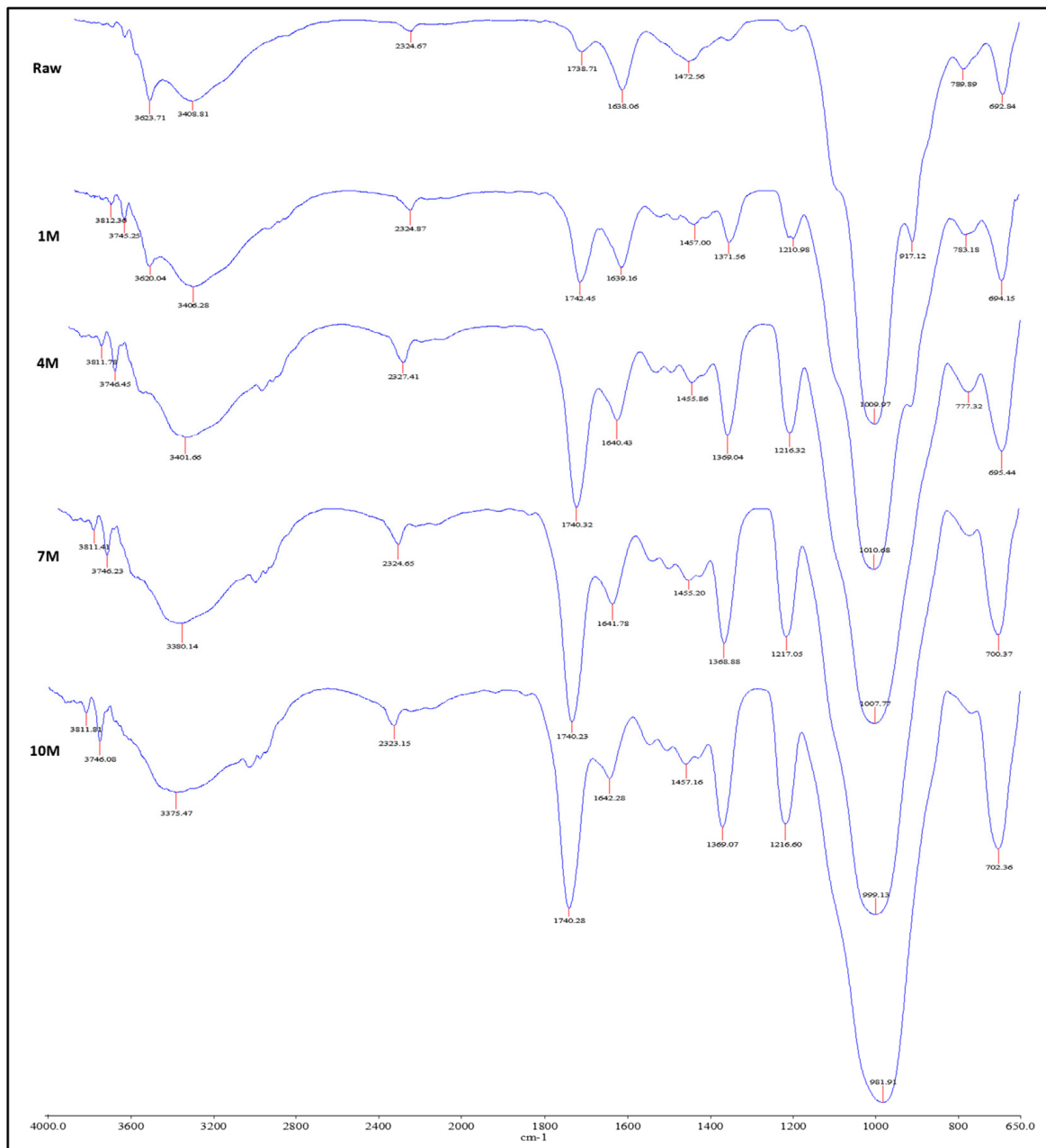

Figure 5. FTIR analysis depicting raw BC and BABC activations (1–10 M).
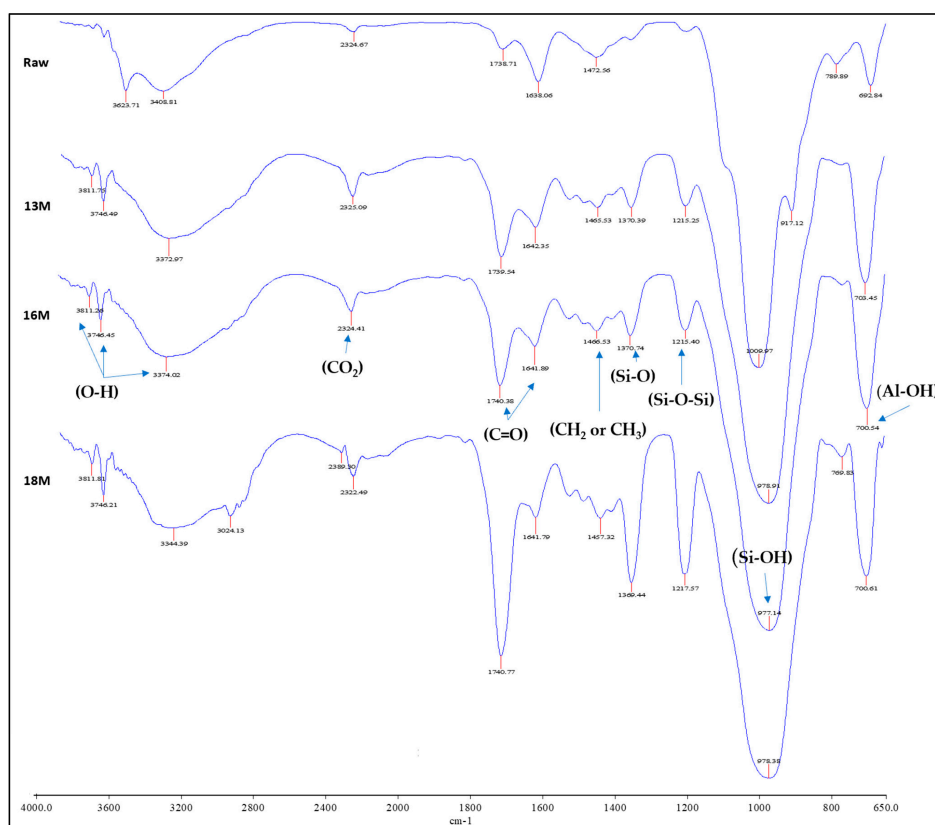
Figure 6. FTIR analysis depicting raw BC and BABC activations (13–18 M).

For NaOH activation, in the Fourier transform infrared (FTIR) analysis, characteristic peaks were observed at specific wavenumbers for different activation dosages (1 M, 4 M, 7 M, 10 M, 13 M, 16 M, and 18 M), providing valuable insights into the adsorption of MB. The recorded peaks included: 3812.36 cm^{-1} and 3745.25 cm^{-1}, suggesting stretching vibrations of hydroxyl groups (O-H) or moisture absorption; 3620.04 cm^{-1} and 3406.28 cm^{-1}, associated with stretching vibrations of hydroxyl groups (O-H) or water molecules; 2324.87 cm^{-1}, potentially indicating the presence of carbon dioxide (CO_2); 1742.45 cm^{-1}, attributed to carbonyl groups (C=O) or other functional groups related to organic compounds [45]; 1639.16 cm^{-1}, corresponding to water bending or C=O stretching vibrations; 1457.00 cm^{-1}, indicating bending vibrations in CH_2 or CH_3 groups; 1371.56 cm^{-1}, possibly corresponding to Si-O bending vibrations; 1210.98 cm^{-1}, related to the stretching vibrations of Si-O-Si bonds; 783.18 cm^{-1}, indicating Si-O-Si stretching vibrations; and 694.15 cm^{-1}, associated with bending vibrations in Al-OH groups [45–47]. These comprehensive findings underscore the significance of employing specific action dosages, with particular attention to 16 M, which consistently exhibited the most prominent peaks, 3811.26 cm^{-1} and 3746.45 cm^{-1} (possible hydroxyl groups), 3374.02 cm^{-1} (hydroxyl group stretching or water molecules), 2324.41 cm^{-1} (carbon dioxide presence), 1740.38 cm^{-1} (carbonyl groups), 1641.89 cm^{-1} (water bending or C=O stretching), 1466.53 cm^{-1} (CH_2 or CH_3 bending), 1370.74 cm^{-1} (Si-O bending), 1215.40 cm^{-1} (Si-O-Si bonds), 977.14 cm^{-1} (Si-OH stretching), and 700.54 cm^{-1} (Al-OH bending), indicative of enhanced adsorption capabilities facilitated by the presence of functional groups such as carbonyl and Si-O stretching vibrations, crucial in the efficient MB adsorption process [45–47]. Figure 6 illustrates the FTIR characterization analysis of AABC at an optimal activation dosage of 7 M.
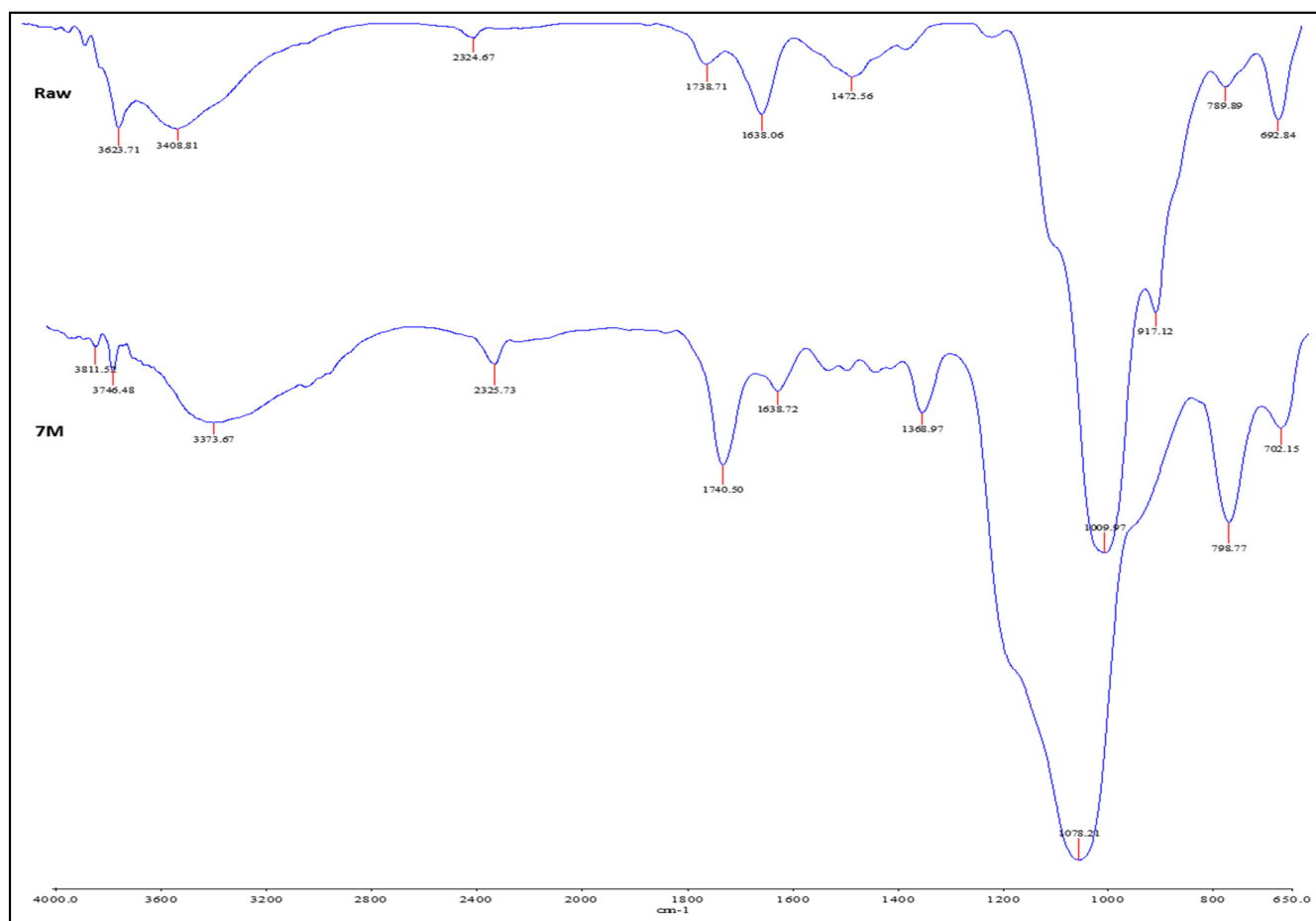
Figure 7. FTIR: raw BC and AACB activation (7 M).

In contrast, for AABC (7 M) activation, peaks at 3811.52 cm^{-1}, 3746.48 cm^{-1}, and 3373.67 cm^{-1} suggested the presence of hydroxyl groups and water molecules. The peak at 2325.73 cm^{-1} indicated the possible presence of CO_2, while peaks at 1740.50 cm^{-1}, 1638.72 cm^{-1}, and 1368.97 cm^{-1} indicated the presence of carbonyl groups, water bending or C=O stretching vibrations, and Si-O bending vibrations. Peaks at 1078.21 cm^{-1}, 798.77 cm^{-1}, and 702.15 cm^{-1} corresponded to stretching vibrations of Si-O bonds, Si-O-Si bonds, and bending vibrations of Al-OH groups, respectively [17,37].

The superiority of the 16 M activation over AABC (7 M) can be attributed to the higher intensity and variety of functional groups identified, particularly those associated with hydroxyl and carbonyl groups, as well as Si-O stretching vibrations. These functional groups are crucial for the adsorption of MB, as they can form hydrogen bonds, electrostatic interactions, and ion exchange with the dye molecules [48,49], enhancing the overall adsorption capacity of BC. Therefore, the 16 M activation dosage offers more favorable conditions for removing MB from aqueous solutions compared to AABC (7 M) activation.

3.1.6. XRD Analysis

X-ray diffraction (XRD) analysis was conducted to assess the crystalline structure of raw bentonite clay (BC) and base-activated bentonite clay (BABC) samples at varying NaOH activation dosages (1 M, 4 M, 7 M, 10 M, 13 M, 16 M, and 18 M), as well as the acid-activated bentonite clay (AABC) at the optimal dosage of 7 M. The diffraction patterns depicted in Figures 8 and 9 for BABC and AABC samples were analyzed at a 2θ diffraction angle by using Xpert HighScore software (version 5.2). Detailed peak data are provided in Table S1 of the Supplementary Section.
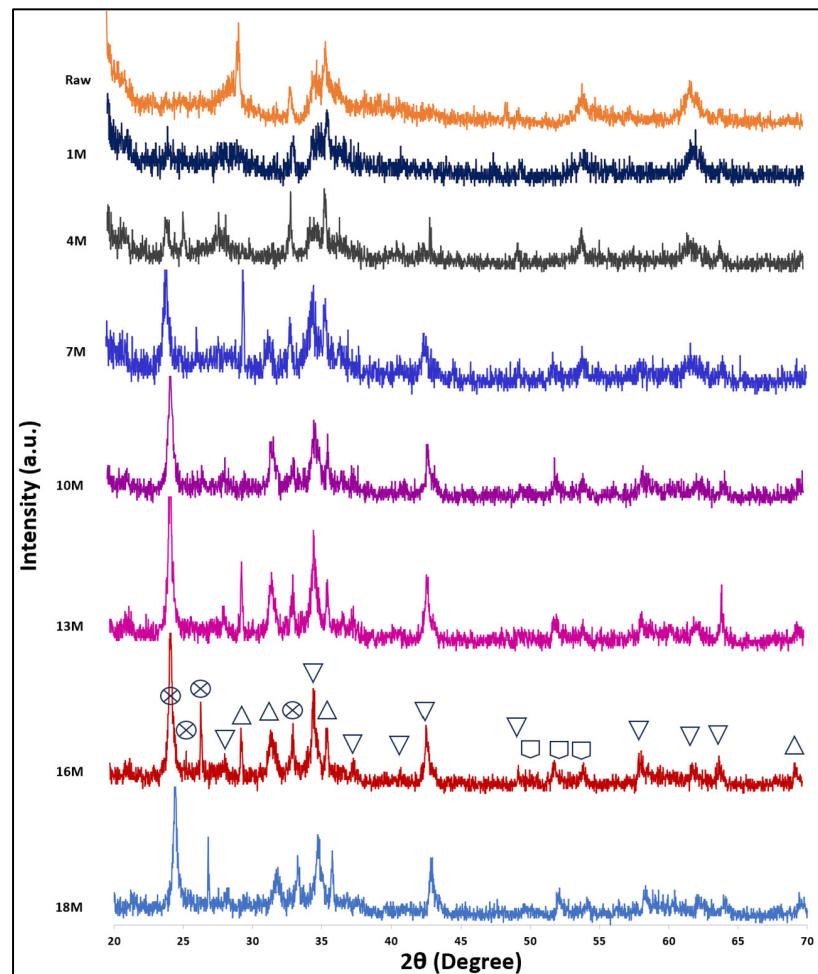
Figure 8. XRD analysis of raw BC and activation (1–18 M) of BABC, (Na$_2$O ($\otimes$), SiO$_2$ ($\triangle$), Al$_2$O$_3$ ($\triangledown$), MgO ($\sqcup$)).
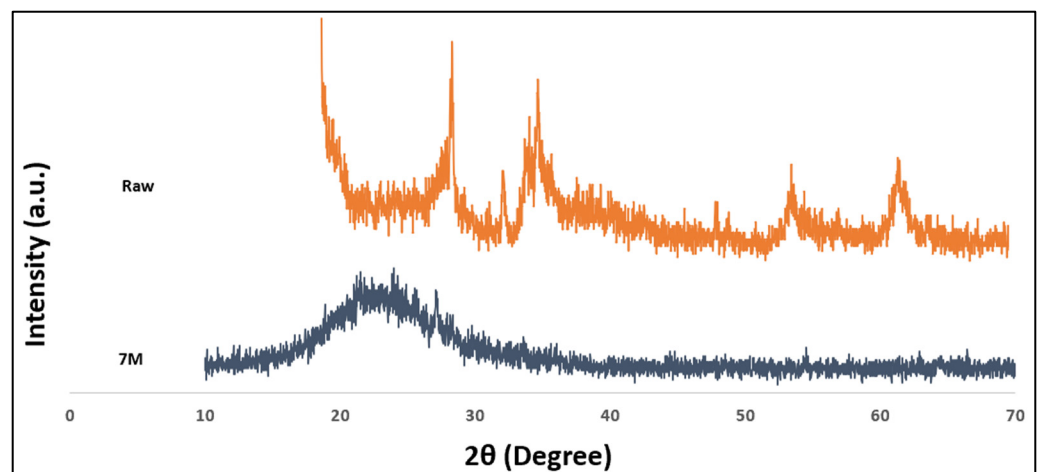
Figure 9. XRD analysis of raw BC and activation (7 M) of AABC.

The analysis revealed that raw BC samples displayed characteristic diffraction peaks at specific angles and intensities, namely 29.48° (134, indicating SiO$_2$), 33.14° (58, indicating Na$_2$O), 35.72° (112, indicating SiO$_2$), 48.62° (40, indicating MgO or Mg-containing compounds), 54.12° (62, indicating Al$_2$O$_3$), and 61.86° (66, indicating SiO$_2$), consistent with the literature [50].

Notably, the XRD pattern of the 16 M activation of BABC in Figure 8 displayed significant peaks at various angles, such as 24.44° (intensity 170, Na_2O ($\otimes$)), 25.52° (intensity 38, Na_2O), and 26.56° (intensity 80, Na_2O), indicative of the increased presence of sodium oxide. Similarly, peaks for aluminum oxide and silicon dioxide, crucial for the adsorption process, showed significant intensities at 28.3° (intensity 36, Al_2O_3), 29.48° (intensity 58, SiO_2 ($\triangle$)), 31.64° (intensity 56, SiO_2), 33.24° (intensity 62, Na_2O), 34.7° (intensity 92, Al_2O_3 ($\triangledown$)), 35.62° (intensity 58, SiO_2), 37.7° (intensity 32, Al_2O_3), 41.04° (intensity 24, Al_2O_3), 42.8° (intensity 60, Al_2O_3), 49.48° (intensity 26, Al_2O_3), 51.98° (intensity 28, MgO ($\cup$)), 52° (intensity 24, MgO), 54.2° (intensity 28, MgO), 58.36° (intensity 38, Al_2O_3), 62.3° (intensity 28, Al_2O_3), 63.98° (intensity 34, Al_2O_3), and 64.42° (intensity 28, SiO_2), these alterations suggest a reconfiguration of the clay matrix conducive to enhanced adsorption properties, particularly for MB removal [39,45].

In contrast, the X-ray diffraction pattern of the optimal activation of AABC (7 M), shown in Figure 9, exhibited distinct peaks at around 23° (intensity 122, SiO_2) and 27.1° (intensity 100, Al_2O_3), attributed to silicon dioxide and aluminum oxide, respectively, aligning with previous findings [46]. Based on the XRD analysis, the 16 M activation condition displayed superior intensities of relevant compounds compared to all BABC and AABC activation dosages, suggesting its enhanced suitability for MB adsorption. This condition is anticipated to offer a higher adsorption capacity for MB than other activation conditions.

The augmentation in peak intensities and the subsequent crystalline enhancement observed in the 16 M NaOH-activated BABC samples can be attributed to the alkaline activation process. This process facilitates the dissolution of silicate structures within the bentonite clay, thereby enabling the leaching of silica and alumina. The re-polymerization of these leached elements forms new aluminosilicate phases characterized by increased surface areas and porosities. This structural evolution is instrumental in the elevated adsorption capacities noted in BABC samples, distinguishing them from their AABC counterparts, which exhibit a more constrained compositional modification due to the acid activation mechanism primarily focusing on the extraction of octahedral cations without significantly promoting the formation of new crystalline phases [51–53].

3.2. Adsorption Experiments

The optimization parameters, encompassing contact time, initial concentration, temperature, pH, and dosage, were evaluated using a UV spectrophotometer (Shimadzu UV-1800, Kyoto, Japan) with a wavelength of 663 nm, following the methodology outlined by [54–56]. Subsequently, the study determined that the most effective activation dosage for MB removal was 16 M of BABC, surpassing all activation dosages of AABC and BABC. This was achieved under specific conditions, including a 24-h duration, a pH of 7, a temperature of 25 °C, an initial concentration of 50 ppm, and a dosage of 0.8 g at 135 rpm in 100 mL.

Acid activation significantly improved adsorption performance, with the highest removal percentage achieved at a 7 M activation dosage. Similarly, base activation enhanced adsorption capacity, reaching its peak at a 16 M dosage. Comparing acid and base activation, base activation demonstrated slightly better final concentration and removal percentage results. Significantly, the 16 M (BABC) showcased outstanding performance, demonstrating accelerated methylene uptake kinetics. It achieved a final concentration of merely 0.078 ppm and an exceptional removal percentage of 99.842%. The superiority of 16 M BABC lies in its enhanced adsorption capacity, attributed to the introduction of hydroxyl (-OH) and carbonyl (C=O) groups, electrostatic attraction, ion exchange, Si-OH, Al-OH, Si-O stretching vibrations, and the formation of micro- and mesopores as presented in Figure 10. Additionally, the activation process introduces negative charges on the clay surface, fostering attractive electrostatic interactions with MB molecules and thus enhancing adsorption efficiency.
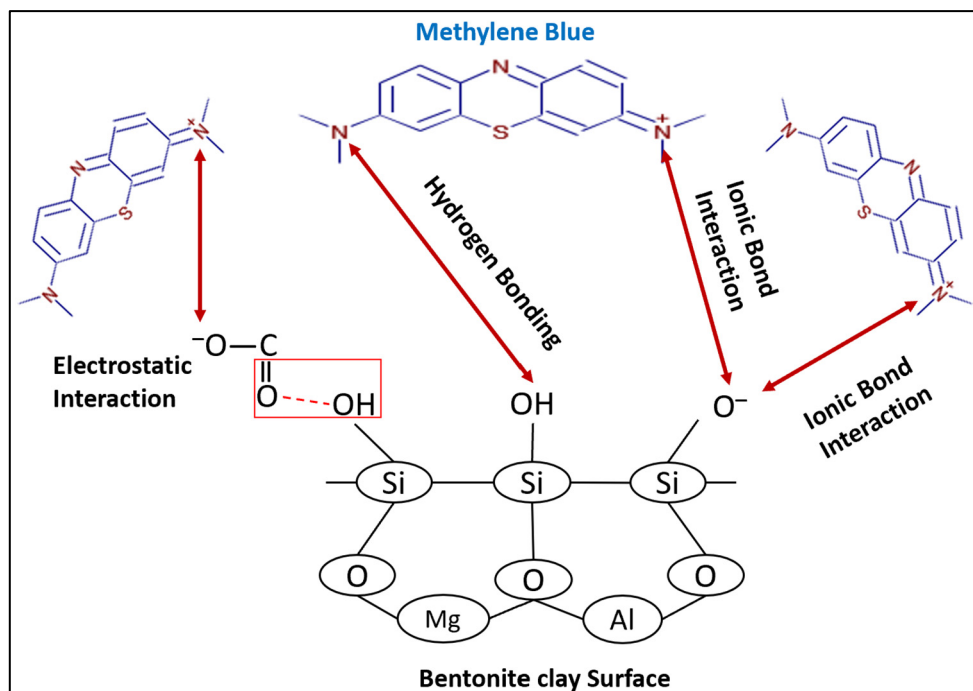
Figure 10. Mechanisms of methylene blue adsorption on BABC.

3.2.1. Effect of Contact Time

The adsorption process was conducted to determine the optimal contact time for removing MB using BC. The experiments were carried out at a constant temperature of 25 °C, pH 7, with a dosage of 0.8 g and an initial concentration of 50 ppm. The contact time was varied from 45 to 315 min, with measurements taken every 45 min using shaker equipment operating at 135 rpm using a shaker (KS 4000 I control (IKA)—Werke GmbH & Co. KG, Staufen, Germany). Figure 11 depicts the optimization investigation, showing changes in contact time and visually representing adsorption capacity (q_e) over time.
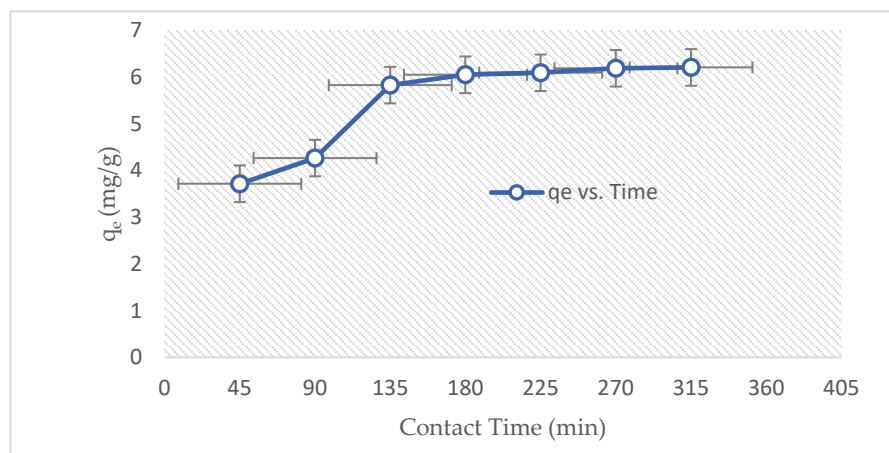
Figure 11. Optimization: contact time (0–315 min, 50 ppm, 25 °C, pH 7, 0.8 g).

By varying the contact time (45, 90, 135, 180, 225, 270, 315 min) while maintaining a constant temperature of 25 °C, pH of 7, 0.8 g dosage, and 50 ppm initial concentration, the most favorable outcomes were observed at 270 min within a 100 mL solution. The MB concentration reached 0.461 ppm at this juncture, showcasing an impressive removal efficiency of 99.077%. The associated adsorption capacity was determined to be 6.192 mg/g, underlining the clay's remarkable affinity for MB. Equilibrium at 300 min was observed (within a range of 20 to 320 min) and achieved a 95% removal of MB, employing conditions

of 200 ppm (mg/L) initial concentration, 1.5 g dosage, pH 8, 150 rpm agitation, and 30 °C in a 50 mL solution [57]. Meanwhile, equilibrium was reached at 360 min, achieving an approximate 90% removal with conditions involving 8 g dosage, pH 9, 22 °C, 500 rpm agitation, and 20 ppm (mg/L) initial concentration in an 800 mL solution [58]. In a separate study, they completed their adsorption within the first 5 h (300 min), utilizing pH 9, 25 °C conditions, and concentrations up to 80 ppm in a 50 mL solution [59].

3.2.2. Effect of Initial Concentration

To assess the influence of initial concentration on the adsorption of MB using BC, experiments were conducted with a fixed contact time of 270 min. The initial concentration of the solution was varied in the range of 50 to 200 ppm while keeping other experimental conditions constant, including a dosage of 0.8 g, a temperature of 25 °C, and a pH of 7. The adsorption process was monitored at 45-min intervals using shaker equipment operating at 135 rpm. Figure 12 presents the optimization analysis, displaying fluctuations in initial concentration and graphically illustrating adsorption capacity (q_e) with respect to initial concentration.
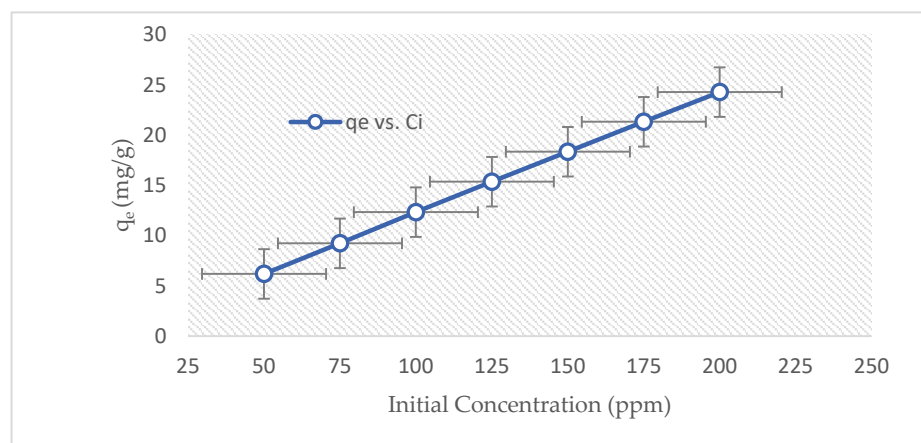
Figure 12. Optimization: initial concentration (75–200 ppm, 270 min, 25 °C, pH 7, 0.8 g).

The influence of initial concentration (ranging from 75 to 200 ppm) on adsorption was explored under conditions of 25 °C, 0.8 g dosage, 270 min contact time, and pH 7. The most favorable outcome emerged at 200 ppm among the various concentrations tested. This concentration yielded a notable result, leading to a considerable reduction in MB's final concentration to 5.652 ppm, showcasing an impressive removal efficiency of 97.173%. The adsorption capacity also reached a remarkable value of 24.293 mg/g. In a similar context, a 95% MB removal rate within 300 min (equivalent to 5 h) was accomplished, utilizing parameters including 200 ppm (mg/L) initial concentration, 1.5 g dosage, pH8, and 30 °C within a 50 mL solution [57]. Moreover, the adsorption of MB onto Na-bentonite clay was delved into. Their study underscored the notable impact of initial concentration on MB's adsorption onto Na-bentonite, revealing an observable rise in adsorption capacity with increasing initial concentration [60].

3.2.3. Effect of Temperature

To investigate the effect of temperature on the adsorption of MB using BC, experiments were conducted while keeping the initial concentration constant at 200 ppm. The temperature range studied varied from 25 to 50 °C, with a fixed contact time of 270 min. Other parameters, including a dosage of 0.8 g and a pH of 7, were maintained throughout the experiments. The adsorption process was monitored using shaker equipment operating at 135 rpm, and measurements were taken at 45-min intervals. Figure 13 showcases the optimization exploration, demonstrating variations in temperature and visually representing adsorption capacity (q_e) with temperature changes.
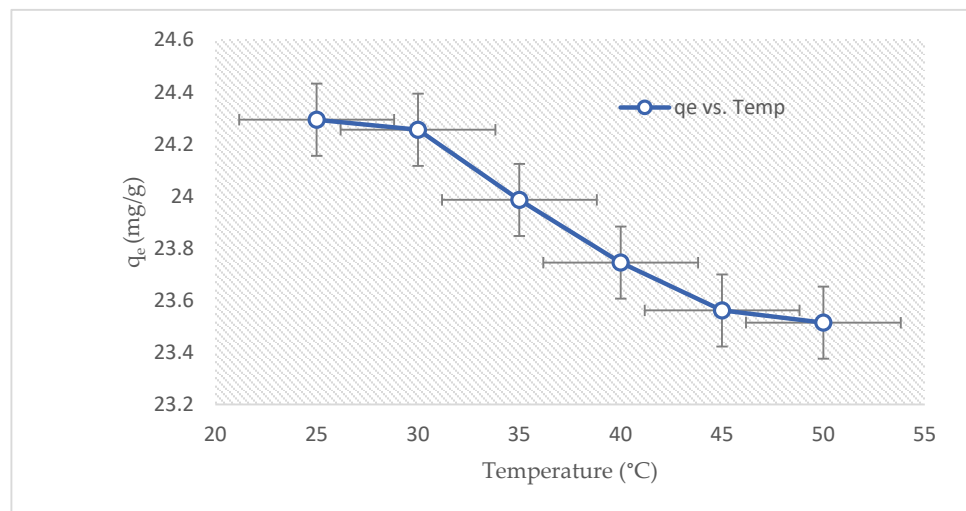
Figure 13. Optimization: temperature (25–50 °C, 270 min, 200 ppm, pH 7, 0.8 g).

The impact of temperature (ranging from 25 to 55 °C) on adsorption was investigated under consistent conditions involving a 0.8 g dosage, pH 7, 200 ppm initial concentration, and 270 min of contact time. Surprisingly, the most favorable outcomes were observed at the lowest tested temperature, 25 °C, aligning with findings from prior research [61,62]. Notably, at this temperature, the final concentration of MB was diminished to 5.652 ppm, signifying a robust removal efficiency of 97.173% and an adsorption capacity of 24.293 mg/g. Additionally, a temperature range of 20 °C to 50 °C was explored, revealing that the removal efficiency escalated as the temperature increased from 20 to 30 °C. Specifically, at 30 °C, the removal percentage reached 95% after 200 min, while achieving a similar removal efficiency necessitated 300 min at 20 °C [57]. Conversely, the removal rate of MB showed marginal improvement at 40 °C and 50 °C when compared to the performance at 30 °C. Correspondingly, temperature ranges of 25 °C to 45 °C were investigated, and it was ascertained that the optimal outcomes were observed at 25 °C [59].

3.2.4. Effect of pH

To assess the influence of pH on the adsorption of MB using BC, a pH range of 4 to 10 was examined while keeping the temperature constant at 25 °C. The contact time was set at 270 min, and other parameters, such as the initial concentration (200 ppm) and dosage (0.8 g), remained unchanged. The adsorption process was monitored using shaker equipment operating at 135 rpm, with measurements taken at 45-min intervals. Figure 14 highlights the optimization inquiry, displaying pH variations and providing a visual representation of adsorption capacity (q_e) at different pH levels.
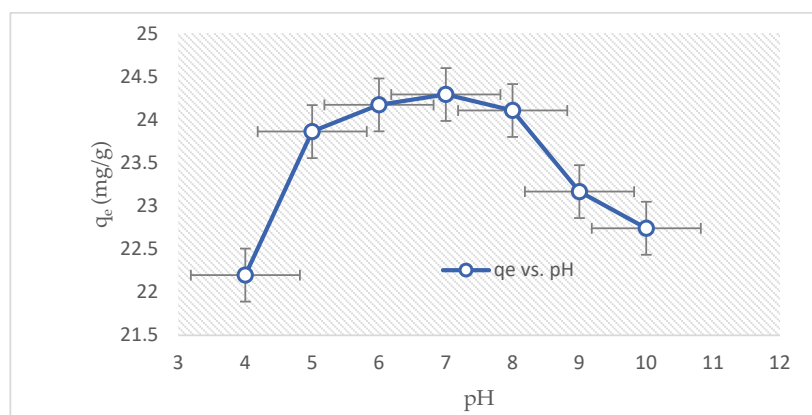

Figure 14. Optimization: pH (4–10 pH, 270 min, 200 ppm, 25 °C, 0.8 g).

The impact of pH levels (ranging from 4 to 10) on the adsorption process was investigated under controlled conditions, including a 200 ppm initial concentration, 270 min of contact time, 25 °C temperature, and a 0.8 g dosage. Notably, the optimal pH was determined to be 7, yielding a final concentration of 5.652 ppm. The exceptional adsorption capacity and removal efficiency at pH 7 are due to optimized surface charge, favorable surface chemistry promoting active functional groups, and ideal solution speciation for MB interaction. These conditions facilitate strong electrostatic interactions and hydrogen bonding between the clay surface and MB molecules, resulting in efficient adsorption. pH 7 represents an optimal balance between surface charge, solution chemistry, and clay-mineral interactions, crucial for maximizing MB removal efficiency, which aligns with findings from prior research [62–64]. This pH-dependent optimization resulted in an impressive removal efficiency of 97.173% and an adsorption capacity of 24.293 mg/g.

3.2.5. Effect of Dosage

To examine the influence of dosage on adsorption, various dosages ranging from 0.5 to 0.95 g were tested while maintaining a pH of 7. The experiments were conducted at a constant temperature of 25 °C, with a contact time of 270 min and an initial concentration of 200 ppm. The adsorption process was monitored using shaker equipment operating at an agitation speed of 135 rpm, with measurements taken at 45-min intervals. Figure 15 emphasizes the optimization research, presenting dosage variations and offering a graphical representation of adsorption capacity (q_e) concerning dosage changes.
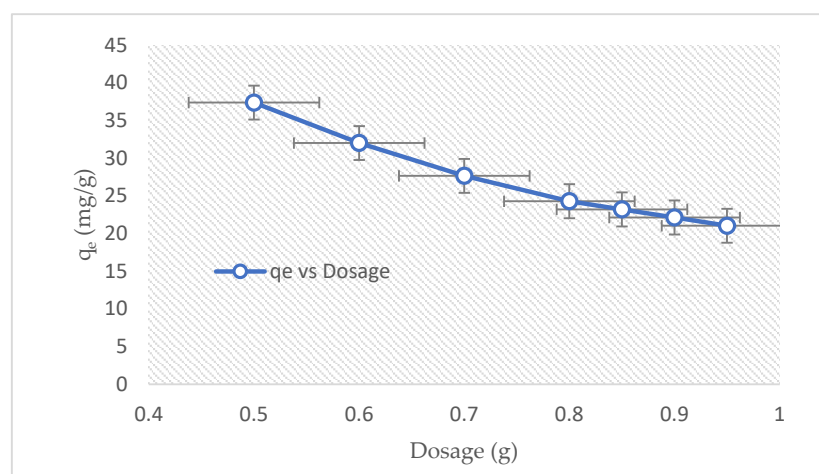

Figure 15. Optimization: dosage (0.5–0.95 g, 270 min, 200 ppm, 25 °C, pH 7).

The results revealed that the dosage of BC played a crucial role in the adsorption of methylene blue. Among the tested dosages (ranging from 0.5 to 0.95 g), a dosage of 0.9 g exhibited the most favorable adsorption performance. At this optimal dosage, the final concentration of MB decreased significantly to 0.130 ppm, demonstrating an impressive removal efficiency of 99.593%. Additionally, the adsorption capacity reached a remarkable value of 21.131 mg/g, highlighting the high adsorption capability of the clay. Exhibiting the clay's notable adsorption prowess, in line with earlier research conducted by [62,65], these findings emphasize the considerable adsorption capabilities of BC as a potent adsorbent for MB elimination. The study underscores the heightened adsorption potential achieved with escalating dosages. However, it also highlights the inherent trade-off between increased capacity and a subsequent decrease in adsorption speed. These findings emphasize the importance of selecting an appropriate dosage for efficient MB removal using BC, with a dosage of 0.9 g proving to be highly effective in achieving desirable adsorption outcomes.

In conclusion, this study successfully optimized the adsorption of MB using BABC, achieving optimal conditions of a contact time of 270 min, an initial concentration of 200 ppm, a temperature of 25 °C, a pH of 7, and a dosage of 0.9g. The BABC demonstrated

a remarkable adsorption capacity of 12 pt-co (0.813 mg/L (ppm)), meeting the WHO drinking water standards of a maximum accepted value of 15 UTC (1UTC = 1 pt-co). These findings highlight the effectiveness of BABC as an adsorbent for MB removal, offering a practical and cost-effective solution for efficient pollutant removal in water treatment applications while adhering to stringent water quality requirements.

3.3. Kinetic Study of Methylene Blue Adsorption

In the exploration of adsorption kinetics, two models, the pseudo-first-order and pseudo-second-order, were applied for data analysis. The pseudo-first-order model demonstrated a satisfactory fit to the experimental data, yielding an R-squared value of 0.9529 and a q_e value of 2.32, as depicted in Figure 16a. This model, predicated on the assumption that the adsorption rate is proportional to the difference between the equilibrium adsorption capacity and the amount of adsorbate adsorbed at a given time, provided meaningful insights. The positive rate constant (K1 = 0.00002) further validates the suitability of the model for our experimental system.
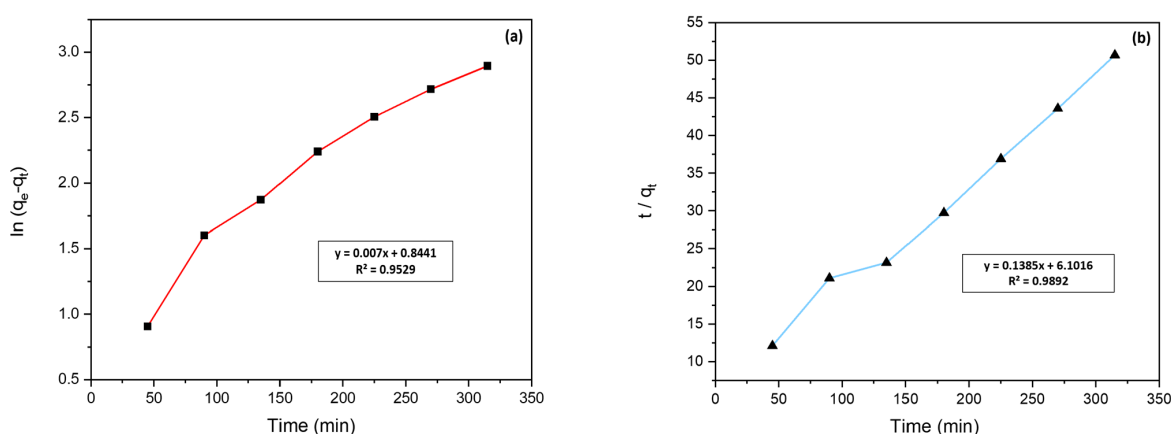

Figure 16. Kinetic model results: (**a**) pseudo-first-order; (**b**) pseudo-second-order (experimental conditions: 315 min, 50–200 ppm, 25 °C, pH 7, 0.8 g).

In contrast, the pseudo-second-order model exhibited an exceptional fit to the experimental data, with an elevated R-squared value of 0.9892 and a q_e value of 7.22, as shown in Figure 16b. This model, which considers the adsorption rate's dependence on the square of the remaining concentration of the adsorbate and is typically associated with chemisorption mechanisms involving strong chemical bonding, provided more profound insights into the adsorption kinetics. The positive rate constant (K2 = 0.003) reinforces the reliability of the model, indicating that the adsorption process is primarily governed by kinetics.

Table 3 and Figure 16 showcase the results from the adsorption kinetic models. The pseudo-second-order model, distinguished by its high R-squared value of 0.9892, provides a more accurate depiction of the adsorption kinetics, aligning with previous research findings [66–71]. Furthermore, this model highlights the chemisorption process, underscoring the robust interactions between the adsorbate and the adsorbent surface.

Table 3. Adsorption kinetic models results under the following conditions: 270 min, 50–200 ppm, 25 °C, pH 7, and 0.8 g.

Model	Parameter	MB
PFO	q_e (mg/g)	2.32
	K1 (L/min)	0.00002
	R^2	0.9529
PSO	q_e (mg/g)	7.22
	K2 (g/mg min)	0.003
	R^2	0.9892

3.4. Isotherm Analysis of Methylene Blue Adsorption

The Langmuir model, renowned for its assumption of monolayer adsorption on a homogeneous surface, was employed to scrutinize the experimental data. The robust R-squared value of 0.9578 underscores its apt fit, suggesting a probable monolayer formation of MB molecules on the BABC. A low adsorption rate constant (KL) value of 0.002 indicates a leisurely adsorption process, while the maximum adsorption capacity (max) of 27.93 signifies the pinnacle adsorbate quantity. This model's reliability is further affirmed by its substantial R-squared value of 0.9582, substantiating its efficacy in elucidating MB adsorption behavior.

Conversely, the Freundlich model, predicated on multilayer adsorption on a heterogeneous surface, fits the experimental data commendably, boasting a high R-squared value of 0.9814 and a calculated KF value of 9.74 with a Freundlich exponent (n) of 1.79. This underscores the model's accuracy in delineating MB adsorption dynamics on the BABC surface, as seen in Figure 17. The elevated KF value suggests heightened adsorption potential, rendering the Freundlich model adept at characterizing the system's adsorption behavior.
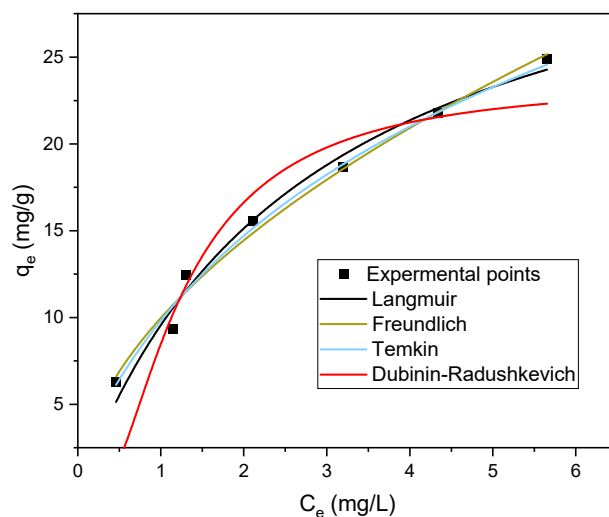

Figure 17. Isotherm model results: (black) Langmuir; (green) Freundlich; (blue) Temkin; (red) Dubinin–Radushkevich (experimental conditions: 270 min, 50–200 ppm, 25 °C, pH 7, 0.8 g).

Furthermore, the Temkin model, which accounts for a non-linear decline in adsorption energy with increased surface coverage, offers a satisfactory fit with a moderate R-squared value of 0.9431. Although its A value of 3.99 signifies the adsorption equilibrium binding constant, the higher R-squared value of the Freundlich model (0.9638) indicates a superior representation of MB adsorption on the clay.

Similarly, the Dubinin–Radushkevich model, exploring adsorption mechanisms and interactions, exhibits a good fit with an R-squared value of 0.8165 but with limitations in capturing the complexity of MB adsorption on the BABC surface.

The adsorption isotherm models, depicted in Figure 17 and Table 4, indicate that the Freundlich isotherm model provides the optimal fit for describing methylene blue (MB) adsorption onto base-activated bentonite clay (BABC). This model's superior alignment and capability to articulate multilayer adsorption processes align with findings from prior studies [66,69–72]. The effectiveness of the Freundlich model in capturing the complexities of MB adsorption enhances the understanding of adsorption dynamics in water treatment applications.

Table 4. The outcomes of adsorption isotherm models under specified experimental conditions (270 min, 200 ppm, 25 °C, 7 pH, and 0.8 g).

Model	Parameter	MB
Langmuir	Q_m (mg/g)	27.93
	K_L (L/mg)	0.002
	R^2	0.9582
Freundlich	K_F (mg/g) $\times$ (L/mg) (1/n)	9.74
	n	1.79
	R^2	0.9814
Temkin	b_T (J/mol)	7.56
	A (L/g)	3.99
	R^2	0.9638
Dubinin–Radushkevich	ε (KJ/mol)	5000,000
	β (mol^2/KJ^2)	2×10^{-7}
	q (mg/g)	19.18
	R^2	0.8165

3.5. Thermodynamic Study

The thermodynamic study, conducted under controlled conditions (270 min contact time, 200 ppm initial concentration, pH 7, 0.8 g dosage), provided insights into MB adsorption onto BABC over a temperature range of 25–50 °C, as shown in Figure 18.
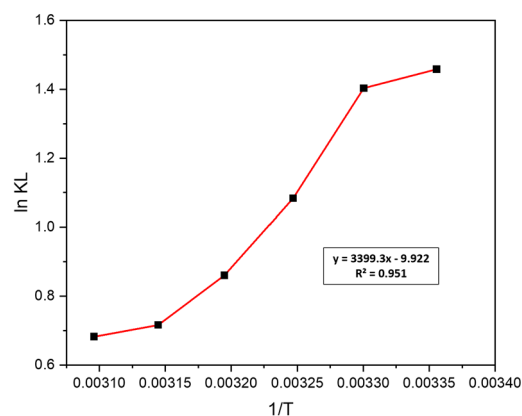
Figure 18. Thermodynamic study of BABC (experimental conditions: 270 min, 200 ppm, 25–50 °C, pH 7, 0.8 g).

Temperature variations from 25 °C to 50 °C revealed a trend where higher temperatures correlated with lower final concentrations of the adsorbate, suggesting enhanced adsorption capacity at lower temperatures, highlighting the importance of temperature control for optimizing adsorption efficiency.

The calculation of Gibbs free energy ($\Delta G°$), enthalpy ($\Delta H°$), and entropy ($\Delta S°$) unveiled crucial thermodynamic characteristics. Negative $\Delta G°$ values (-3.61 to -1.83) indicated the spontaneity and favorability of adsorption across the temperature range, regardless of fluctuations.

Moreover, the negative $\Delta H°$ (-28.26) signified an exothermic adsorption process with heat release, consistent with prior findings. The negative $\Delta S°$ (-82.49) suggested reduced disorderliness during adsorption, indicating a transition to more ordered states. Table 5 illustrates the outcomes of the thermodynamic study.

Table 5. Thermodynamic study results under specified conditions (270 min, 200 ppm, 25–55 °C, 7 pH, and 0.8 g).

Adsorbate	ΔH (KJ/mol)	ΔS (KJ/mol)	ΔG (KJ/mol)					
			25 °C	30 °C	35 °C	40 °C	45 °C	50 °C
MB	−28.26	−82.49	−3.61	−3.53	−2.77	−2.23	−1.89	−1.83

In essence, the study revealed a spontaneous, exothermic adsorption process with decreased entropy, emphasizing the importance of considering thermodynamic parameters in optimizing adsorption processes for water treatment, consistent with previous studies [62,73].

3.6. Regeneration and Reusability

The BABC regeneration study aimed to restore its adsorption capacity using four techniques. The clay was stirred at 80 °C and 15 rpm for varying durations (1 and 2 h) using a specific volume ratio of sodium persulfate (0.1:0.2). Sample 1 was regenerated with 70 mL for 1 h, Sample 2 with 70 mL for 2 h, Sample 3 with 250 mL for 1 h, and Sample 4 with 250 mL for 2 h. The regenerated adsorbents were used in a subsequent adsorption study under the same optimization conditions as the initial experiment (0.9 g, 25 °C, 200 ppm, 270 min, and pH 7), as illustrated in Figure 19. These results provide valuable insights into the regenerative capacity and reusability of the BABC for sustained removal of MB.
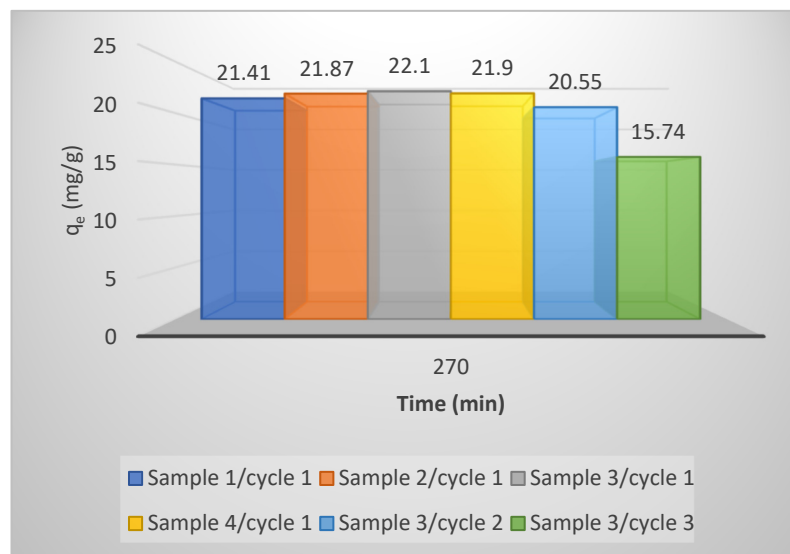
Figure 19. All regeneration and reusability cycle results (experimental conditions: 270 min, 200 ppm, 25 °C, pH 7, 0.9 g).

Four techniques were evaluated, and sample 3, with a larger volume and shorter treatment duration, showed the best performance in terms of final concentration, adsorption capacity, and removal efficiency. Nonetheless, it is essential to highlight that the effectiveness of the regenerated adsorbent progressively declined with each successive cycle, consistent with earlier investigations conducted by [74,75]. These studies demonstrated a decrease in the percentage removal of MB with each recycling cycle. In the second and third cycles, there was a noticeable decrease in adsorption capacity and reduction efficiency, aligning with the findings of [74], which achieved approximately 95% removal over three cycles using 100 ppm, pH 7, and 70 °C. This decline can be attributed to factors such as incomplete restoration of the adsorbent's properties during regeneration, surface saturation, or fouling due to repeated usage.

3.7. Surface Characterization of BABC Pre- and Post-MB Adsorption

3.7.1. FTIR Analysis

FTIR analysis was carried out to explore alterations in the surface of BABC during MB adsorption and subsequent regeneration and reusability, as depicted in Figure 20. The obtained spectra revealed characteristic peaks associated with various functional groups on the clay surface.
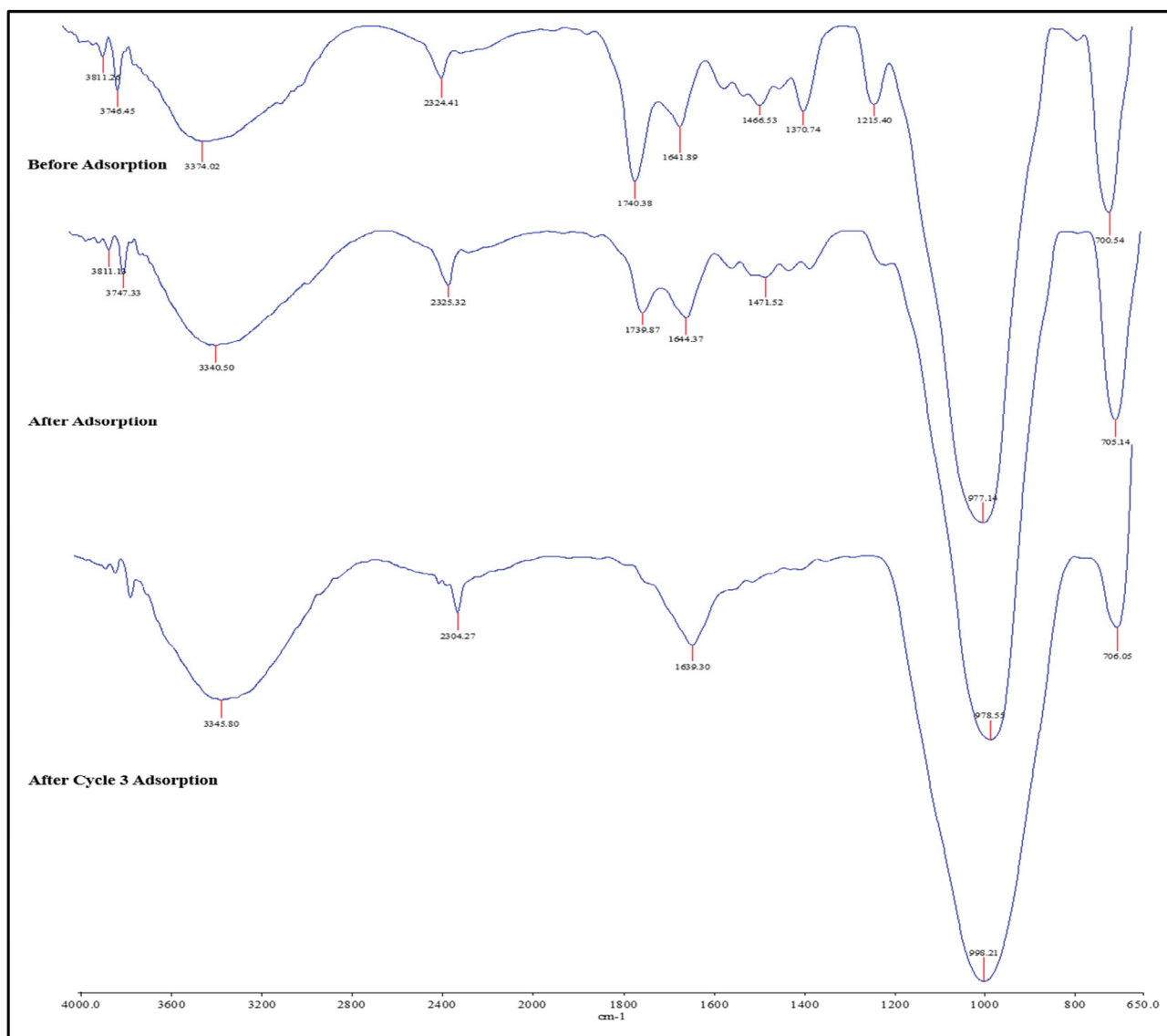

Figure 20. FTIR: Before, after, and after cycle 3 adsorption of BABC.

Before adsorption, the FTIR spectrum of the BABC displayed distinctive peaks, including peaks at 3811.26 cm^{-1} (X group), 3746.45 cm^{-1} (Y group), 3374.02 cm^{-1} (Z group), and 2324.41 cm^{-1} (W group), indicating the presence of these functional groups. Additional peaks at 1740.38 cm^{-1}, 1641.89 cm^{-1}, and 1466.53 cm^{-1} were assigned to specific functional groups [45].

Following the adsorption process, changes in the FTIR spectrum indicated interactions between MB and the clay surface. The shifts and intensity variations in peaks, particularly at 3811.13 cm^{-1}, 3747.33 cm^{-1}, and 3340.50 cm^{-1}, suggested the involvement of X, Y, and Z groups in the adsorption of methylene blue.

After the regeneration and reusability processes, further changes in the FTIR spectrum were observed. The shifts and intensity variations in peaks indicated the removal of

adsorbed MB and the restoration of functional groups on the clay surface. New peaks at 3345.80 cm^{-1}, 2304.27 cm^{-1}, 1639.30 cm^{-1}, 998.21 cm^{-1}, and 706.05 cm^{-1} emerged, indicating the reformation of specific functional groups on the clay surface [45–47].

The observed changes in the FTIR spectra confirmed the successful adsorption of MB on the BABC and the involvement of specific functional groups in the process. These findings provided valuable evidence supporting the efficacy of the adsorption process and the successful regeneration and reuse of the BABC. Identifying the specific functional groups involved contributes to a deeper understanding of the underlying mechanisms and aids in optimizing the adsorption process.

3.7.2. BET Analysis

Surface area analysis of the BABC material was conducted utilizing the BET method. This analysis aimed to ascertain alterations in the surface area resulting from all MB adsorption processes, as outlined in Table 6.

Table 6. Surface area, pore volume, and size of BABC before, after, and after regeneration and reusability cycle 3 adsorption.

BABC	Surface Area (m^2/g)	Pore Volume (cm^3/g)	Pore Size (Å)
Before Adsorption	74.14	1.11	300.20
After Adsorption	73.1430	0.668	182.726
After Cycle 3	53.86	0.479	136.543

The initial characteristics of the BABC included a surface area of 74.15 m^2/g, a pore volume of 1.11 cm^3/g, and a pore size of 300.20 Å. After methylene blue adsorption, the surface area decreased slightly to 73.1430 m^2/g, while the pore volume was reduced to 0.668 cm^3/g and the pore size decreased to 182.726 Å.

Following the third regeneration cycle and reusability, the BABC exhibited a surface area of 53.86 m^2/g, a pore volume of 0.479 cm^3/g, and a pore size of 136.543 Å.

These changes indicate a decrease in surface area, pore volume, and pore size compared to the initial characteristics. This is likely due to the occupation of surface sites and pore filling by the MB dye molecules. The interaction between the dye and the clay surface may have induced structural modifications, reducing pore size.

Overall, the observed alterations in surface area, pore volume, and pore size align with the expected outcomes of the adsorption process, which correspond to previous studies [74–76], highlighting the influence of MB adsorption on the clay's porosity and surface properties.

Table 7 delineates a side-by-side comparison of our study's effectiveness in methylene blue removal against the backdrop of previous research, highlighting the innovative strategies and outcomes achieved.

Table 7. Comparison of methylene blue removal of adsorbent-based clay minerals.

Substance	BET (m^2/g)	Vol (mL)	Agitation (rpm)	Time (min)	C_i (mg/L)	Temp (C)	pH	Dose (g)	Removal (%)	q_e (mg/g)	Isotherm/ Kinetic	Cycle/ Removal %	Ref.
Bentonite clay (NaOH)	74.15	100	135	270	200	25	7	0.9	99.59	22.131	Freundlich/ second	3/70.8	Current study
MBC (H$_2$SO$_4$/clay)	-	200	140	24 h	300	30	12	0.2	-	34.652	Freundlich/ second	-	[71]
Kaolinite (H$_2$SO$_4$)	76.86	50	150	20	20	-	-	0.2	-	3.40	Langmuir/ Ho-McKay	-	[77]
Malaysian kaolinite (HCl)	-	15	2500	60	20–70	25	6	-	96	1.35–1.37	Freundlich/ second	-	[70]
SG SG-ES SG-SI	633 360 330	40	-	80	10	25	7	0.25	86 80 57	34.3 32.0 22.8	Freundlich/ second	-	[78]

Table 7. *Cont.*

Substance	BET (m²/g)	Vol (mL)	Agitation (rpm)	Time (min)	C_i (mg/L)	Temp (C)	pH	Dose (g)	Removal (%)	q_e (mg/g)	Isotherm/ Kinetic	Cycle/ Removal %	Ref.
clay composite/TiO₂	-	50	150	300	200	30	8	1.5	95	6.3	Langmuir/ second	6/90	[57]
Pure Kaolin (NaOH)	-	100	-	3hrs	12	27	10	0.8	100	20.49	Freundlich	-	[79]
Palygorskite clay (NH₄Cl)	92	40	3000	60	60 100 100	25	9	0.3 0.3 0.5	99.5 78 89	5 ppm/ 40 mg/g–20 ppm/51 mg/g	Langmuir/ second	-	[80]
Bentonite (TiO₂)	-	25	-	45 60 80	10 60 60	25	7	0.15	100 90 100	1.67 7 10	Langmuir/ second	10 ppm/ 10 cycle	[81]
Kaolin Composite	-	800	750	360	20	22	9	8	90	-	Freundlich/ first	-	[58]

4. Conclusions

In conclusion, the study demonstrates that NaOH activation significantly enhances the adsorptive qualities of bentonite clay, transforming it into a base-activated bentonite clay (BABC) distinguished by its mesoporous structure with remarkable adsorptive properties. Detailed characterization revealed BABC's enhanced surface area (74.15 m²/g) and confirmed its superior performance in methylene blue (MB) removal, achieving an impressive efficiency of 99.60% and an adsorption capacity of 22.133 mg/g. The adsorption process, characterized as spontaneous and exothermic, was optimally described by the Freundlich isotherm and pseudo-second-order kinetic model, attesting to BABC's effective adsorption dynamics. Additionally, BABC's ability to maintain high efficiency over three regeneration cycles underscores its viability as a sustainable, cost-effective solution for water treatment, meeting WHO standards for safe water. This study advances our understanding of BABC's potential in MB removal and positions NaOH-activated bentonite clay as a formidable contender in the quest for efficient water purification technologies, marking a significant step forward in environmental remediation efforts.

Supplementary Materials: The following supporting information can be downloaded at: https://www.mdpi.com/article/10.3390/pr12040738/s1, Table S1: XRD analysis illustrating the characteristics of raw BC, BABC (1–18 M), and the optimal AABC activation sample (7 M).

Author Contributions: Conceptualization, H.N.H. and S.I.; methodology, H.N.H., A.A. and S.S.; validation, S.I.; formal analysis, H.N.H. and A.M.A.W.; investigation, H.N.H.; resources, S.I.; data curation, S.I.; writing—original draft preparation, H.N.H.; writing—review and editing, S.I., A.A., S.S. and A.M.A.W.; visualization, S.I.; supervision, S.I., B.Y. and N.S.J. All authors have read and agreed to the published version of the manuscript.

Data Availability Statement: Data are contained within the article and Supplementary Materials.

Conflicts of Interest: The authors declare no conflict of interest.

References

1. Seyrek, M.; Boran, F.; Okutan, M. Treatment of Automotive Paint Wastewater: Photocatalytic degradation of methylene blue using semi-conductive ZrO₂. *Int. J. Automot. Sci. Technol.* **2023**, *7*, 316–324.
2. Sultana, B. Degradation of Dyes Used in Textile Industries by Bacteria Isolated from Local Textile Effluents. Doctoral Dissertation, BRAC University, Dhaka, Bangladesh, 2017.

3. Affat, S.S. Classifications, Advantages, Disadvantages, Toxicity Effects of Natural and Synthetic Dyes: A review. *UTJ Sci.* **2021**, *8*, 130–135.

4. Ouedrhiri, A.; Lghazi, Y.; Bahar, J.; Himi, M.A.; El Haimer, C.; Youbi, B.; Khoukhi, M.; Bimaghra, I. Adsorption of the Methylene Blue Dye in Environmental Water Samples by Biochar Obtained from the Valorization of Argan Shells. *Phys. Chem. Res.* **2022**, *10*, 301–313.

5. Varsha, M.; Senthil Kumar, P.; Senthil Rathi, B. A review on recent trends in the removal of emerging contaminants from aquatic environment using low-cost adsorbents. *Chemosphere* **2022**, *287*, 132270. [CrossRef] [PubMed]

6. Hamad, H.N.; Idrus, S. Recent Developments in the Application of Bio-Waste-Derived Adsorbents for the Removal of Methylene Blue from Wastewater: A Review. *Polymers* **2022**, *14*, 783. [CrossRef]

7. Abegunde, S.M.; Idowu, K.S.; Adejuwon, O.M.; Adeyemi-Adejolu, T. A review on the influence of chemical modification on the performance of adsorbents. *Resour. Environ. Sustain.* **2020**, *1*, 100001. [CrossRef]

8. Anastopoulos, I.; Bhatnagar, A.; Hameed, B.H.; Ok, Y.S.; Omirou, M. A review on waste-derived adsorbents from sugar industry for pollutant removal in water and wastewater. *J. Mol. Liq.* **2017**, *240*, 179–188. [CrossRef]

9. Mohammed, M.A.; Shitu, A.; Ibrahim, A. Removal of Methylene Blue Using Low Cost Adsorbent: A Review. *Res. J. Chem. Sci. ISSN* **2014**, *2231*, 606X.

10. Shahrokhi-Shahraki, R.; Benally, C.; El-Din, M.G.; Park, J. High efficiency removal of heavy metals using tire-derived activated carbon vs commercial activated carbon: Insights into the adsorption mechanisms. *Chemosphere* **2021**, *264*, 128455. [CrossRef]

11. Amin, M.T.; Alazba, A.A.; Shafiq, M. Adsorptive removal of reactive black 5 from wastewater using bentonite clay: Isotherms, kinetics and thermodynamics. *Sustainability* **2015**, *7*, 15302–15318. [CrossRef]

12. Segun Esan, O. The Removal of Single and Binary Basic Dyes from Synthetic Wastewater Using Bentonite Clay Adsorbent. *Am. J. Polym. Sci. Technol.* **2019**, *5*, 16. [CrossRef]

13. Rouhani, H.; Farhadi, F.; Akbari Kenari, M.; Eskandari, E.; Ramakrishna, S. Selection of suitable bentonite and the influence of various acids on the preparation of a special clay for the removal of trace olefins from aromatics. *Clay Miner.* **2021**, *56*, 185–196. [CrossRef]

14. Wan, D.; Li, W.; Wang, G.; Chen, K.; Lu, L.; Hu, Q. Adsorption and heterogeneous degradation of rhodamine B on the surface of magnetic bentonite material. *Appl. Surf. Sci.* **2015**, *349*, 988–996. [CrossRef]

15. Faridah, M.M.; Wan Ibrahim, W.A.; Nodeh, H.R.; Sutirman, Z.A.; Ting, N.N.; Sanagi, M.M. Recent advances in the preparation of oil palm waste-based adsorbents for removal of environmental pollutants—A review. *Malays. J. Anal. Sci.* **2018**, *22*, 175–184. [CrossRef]

16. Tebeje, A.; Worku, Z.; Nkambule, T.T.I.; Fito, J. Adsorption of chemical oxygen demand from textile industrial wastewater through locally prepared bentonite adsorbent. *Int. J. Environ. Sci. Technol.* **2022**, *19*, 1893–1906. [CrossRef]

17. Gandhi, D.; Bandyopadhyay, R.; Soni, B. Naturally occurring bentonite clay: Structural augmentation, characterization and application as catalyst. *Mater. Today Proc.* **2022**, *57*, 194–201. [CrossRef]

18. Noyan, H.; Önal, M.; Sarikaya, Y. The effect of sulphuric acid activation on the crystallinity, surface area, porosity, surface acidity, and bleaching power of a bentonite. *Food Chem.* **2007**, *105*, 156–163. [CrossRef]

19. Önal, M.; Sarikaya, Y. Preparation and characterization of acid-activated bentonite powders. *Powder Technol.* **2007**, *172*, 14–18. [CrossRef]

20. Yener, N.; Bier, C.; Önal, M.; Sarikaya, Y. Simultaneous determination of cation exchange capacity and surface area of acid activated bentonite powders by methylene blue sorption. *Appl. Surf. Sci.* **2012**, *258*, 2534–2539. [CrossRef]

21. Info, A. Effect of Activation Factors on Adsorption of Methylene Blue by Modified Bentonite. *Prog. Color Colorants Coat.* **2013**, *6*, 97–108.

22. Amran, F.; Zaini, M.A.A. Sodium hydroxide-activated Casuarina empty fruit: Isotherm, kinetics and thermodynamics of methylene blue and congo red adsorption. *Environ. Technol. Innov.* **2021**, *23*, 101727. [CrossRef]

23. Jais, F.M.; Chee, C.Y.; Ismail, Z.; Ibrahim, S. Experimental design via NaOH activation process and statistical analysis for activated sugarcane bagasse hydrochar for removal of dye and antibiotic. *J. Environ. Chem. Eng.* **2021**, *9*, 104829. [CrossRef]

24. Kumar, A.; Lingfa, P. Base-Activated Sodium Bentonite Clay: Mutated Characteristics and Industrial Slant. *ECS Trans.* **2022**, *107*, 2303. [CrossRef]

25. Ibrahim, A.S.; Al-Bidry, M.A. Activation Iraqi bentonite for using as drilling mud. *IOP Conf. Ser. Mater. Sci. Eng.* **2019**, *579*, 012006. [CrossRef]

26. Nasuha, N.; Hameed, B.H. Adsorption of methylene blue from aqueous solution onto NaOH-modified rejected tea. *Chem. Eng. J.* **2011**, *166*, 783–786. [CrossRef]

27. Cazetta, A.L.; Vargas, A.M.M.; Nogami, E.M.; Kunita, M.H.; Guilherme, M.R.; Martins, A.C.; Silva, T.L.; Moraes, J.C.G.; Almeida, V.C. NaOH-activated carbon of high surface area produced from coconut shell: Kinetics and equilibrium studies from the methylene blue adsorption. *Chem. Eng. J.* **2011**, *174*, 117–125. [CrossRef]

28. Tabassum, M.; Bardhan, M.; Novera, T.M.; Islam, M.A.; Hadi Jawad, A.; Islam, M.A. NaOH-Activated Betel Nut Husk Hydrochar for Efficient Adsorption of Methylene Blue Dye. *Water Air Soil Pollut.* **2020**, *231*, 398. [CrossRef]

29. Wang, W.; Liu, Y.Y.; Chen, X.F.; Song, S.X. Facile Synthesis of NaOH-modified Fishbone Charcoal (FBC) with Remarkable Adsorption towards Methylene Blue. *Procedia Eng.* **2018**, *211*, 495–505. [CrossRef]

30. Amari, A.; Chlendi, M.; Gannouni, A.; Bellagi, A. Optimised activation of bentonite for toluene adsorption. *Appl. Clay Sci.* **2010**, *47*, 457–461. [CrossRef]

31. Elfadly, A.M.; Zeid, I.F.; Yehia, F.Z.; Abouelela, M.M.; Rabie, A.M. Production of aromatic hydrocarbons from catalytic pyrolysis of lignin over acid-activated bentonite clay. *Fuel Process. Technol.* **2017**, *163*, 1–7. [CrossRef]

32. Wang, J.; Guo, X. Adsorption isotherm models: Classification, physical meaning, application and solving method. *Chemosphere* **2020**, *258*, 127279. [CrossRef]

33. Hashem, A.; Mim, S.; Payel, S.; Rahman, S.; Mizan, A.; Basaran, B.; Nail, A.; Sarker, M.I. Bioresource Technology Reports Thermally activated adsorbent over chemically modified Carica papaya tree adsorbents for removal of chromium from tannery wastewater. *Bioresour. Technol. Rep.* **2024**, *25*, 101692. [CrossRef]

34. Shi, Q.; Wang, W.; Zhang, H.; Bai, H.; Liu, K.; Zhang, J.; Li, Z.; Zhu, W. Porous biochar derived from walnut shell as an efficient adsorbent for tetracycline removal. *Bioresour. Technol.* **2023**, *383*, 129213. [CrossRef]

35. Ezzati, R. Derivation of Pseudo-First-Order, Pseudo-Second-Order and Modified Pseudo-First-Order rate equations from Langmuir and Freundlich isotherms for adsorption. *Chem. Eng. J.* **2020**, *392*, 123705. [CrossRef]

36. Ichou, A.A.; Benhiti, R.; Abali, M.; Dabagh, A.; Chiban, M.; Zerbet, M.; Carja, G.; Sinan, F. Adsorption of pb(Ii) from aqueous solutions onto mgfeal-co3 ldh: Thermodynamic and kinetic studies. *Desalin. Water Treat.* **2020**, *178*, 193–202. [CrossRef]

37. Elnaggar, K.; Farouk, S.; Abdelrazek, A.; Abdelsamie, A.; Ghallab, A.; Mohamed, B.; Elsayed, K.; Ramadan, Y. Optimization, and Characterization of Acid-Activated Bentonite. *Int. J. Ind. Sustain. Dev.* **2022**, *3*, 66–75. [CrossRef]

38. Sarikaya, Y. The Effect of Thermal Treatment on Some of the Physicochemical Properties of a Bentonite. *Clays Clay Miner.* **2000**, *48*, 557–562. [CrossRef]

39. Hebbar, R.S.; Isloor, A.M.; Prabhu, B.; Inamuddin; Asiri, A.M.; Ismail, A.F. Removal of metal ions and humic acids through polyetherimide membrane with grafted bentonite clay. *Sci. Rep.* **2018**, *8*, 4665. [CrossRef]

40. Gumede, S.; Musonge, P. Characterisation of Mg-Al Hydrotalcite and Surfactant-Modified Bentonite Nano Clays for the Treatment of Acid Mine Drainage. *Sustainability* **2022**, *14*, 9501. [CrossRef]

41. Hamah Sor, N.; Mermerdas, K.; Alzeebaree, R.; Ekmen, Ş.; Mulapeer, E.S. Microstructural and Hardened Characteristics of Sustainable High-Performance Alkali-Activated Mortar with Binary Blends of GGBFS and Earth Materials. 2023. Available online: https://papers.ssrn.com/sol3/papers.cfm?abstract_id=4570559 (accessed on 23 February 2024).

42. Slaný, M.; Kuzielová, E.; Žemlička, M.; Matejdes, M.; Struhárová, A.; Palou, M.T. Metabentonite and metakaolin-based geopolymers/zeolites: Relation between kind of clay, calcination temperature and concentration of alkaline activator. *J. Therm. Anal. Calorim.* **2023**, *148*, 10531–10547. [CrossRef]

43. Boudia, R.A.; Bendeddouche, C.K.; Mazari, M.M.; Ech-Chergui, A.N.; Zoukel, A.; Adjdir, M. Zeolite GIS polymorphs derived from clay fraction> 2 μm: The ability of clay fraction> 2 μm for crystallization of high-purity Na-P1 zeolite. *Silicon* **2023**, *15*, 5263–5270. [CrossRef]

44. Kelechukwu, C.; Akaranta, O. Removal of Colorants Using Locally Activated Bentonite Clay: A Review. *IOSR J.* **2021**, *15*, 127574.

45. Ravindra Reddy, T.; Kaneko, S.; Endo, T.; Lakshmi Reddy, S. Spectroscopic Characterization of Bentonite. *J. Lasers Opt. Photonics* **2017**, *4*, 3. [CrossRef]

46. Tabak, A.; Yilmaz, N.; Eren, E.; Caglar, B.; Afsin, B.; Sarihan, A. Structural analysis of naproxen-intercalated bentonite (Unye). *Chem. Eng. J.* **2011**, *174*, 281–288. [CrossRef]

47. Verma, A.; Riaz, U. Sonolytically intercalated poly(anisidine-co-toluidine)/bentonite nanocomposites: pH responsive drug release characteristics. *J. Drug Deliv. Sci. Technol.* **2018**, *48*, 49–58. [CrossRef]

48. Hu, Y.; Guo, T.; Ye, X.; Li, Q.; Guo, M.; Liu, H.; Wu, Z. Dye adsorption by resins: Effect of ionic strength on hydrophobic and electrostatic interactions. *Chem. Eng. J.* **2013**, *228*, 392–397. [CrossRef]

49. Zarroug, S.; Ben Mahmoud, S.; Hamzaoui, A.H.; Essafi, W. Study of the interaction between methylene blue dye and quenched polyelectrolyte with tunable hydrophobicity in aqueous media. *J. Environ. Chem. Eng.* **2019**, *7*, 103312. [CrossRef]

50. Durowaye, S.I.; Sekunowo, O.I.; Lawal, A.I.; Ojo, O.E. Development and characterisation of iron millscale particle reinforced ceramic matrix composite. *J. Taibah Univ. Sci.* **2017**, *11*, 634–644. [CrossRef]

51. Bumanis, G.; Vaičiukynienė, D. Alkali Activation of Milled Red Brick Waste and Calcined Illite Clay with Silica Gel Addition. *Materials* **2022**, *15*, 3195. [CrossRef]

52. Vezentsev, A.I.; Volovicheva, N.A.; Korol'kova, S.V.; Sokolovskiy, P.V. Effect of the Acidic and Alkaline Activation of Bentonite-Like Clays on Sorption Properties in Relation to Fe3+ Ions under Static Conditions. *Russ. J. Phys. Chem. A* **2022**, *96*, 381–386. [CrossRef]

53. Khalifa, A.Z.; Cizer, Ö.; Pontikes, Y.; Heath, A.; Patureau, P.; Bernal, S.A.; Marsh, A.T.M. Advances in alkali-activation of clay minerals. *Cem. Concr. Res.* **2020**, *132*, 106050. [CrossRef]

54. Bhuyan, M.M.; Dafader, N.C.; Hara, K.; Okabe, H.; Hidaka, Y.; Rahman, M.M.; Khan, M.M.R.; Rahman, N. Synthesis of Potato Starch-Acrylic-Acid Hydrogels by Gamma Radiation and Their Application in Dye Adsorption. *Int. J. Polym. Sci.* **2016**, *2016*, 9867859. [CrossRef]

55. Khairnar, S.D.; Shrivastava, V.S. Photocatalytic degradation of chlorpyrifos and methylene blue using α-Bi$_2$O$_3$ nanoparticles fabricated by sol–gel method. *SN Appl. Sci.* **2019**, *1*, 762. [CrossRef]

56. Khosa, M.A.; Shah, S.S.; Nazar, M.F. Application of micellar enhanced ultrafiltration for the removal of methylene blue from aqueous solution. *J. Dispers. Sci. Technol.* **2011**, *32*, 260–264. [CrossRef]

57. Aljar, M.A.A.; Rashdan, S.; El-fattah, A.A. Environmentally Friendly Polyvinyl Alcohol—Alginate/Bentonite Semi-Interpenetrating Polymer Network Nanocomposite Hydrogel Beads as an Efficient Adsorbent for the Removal of Methylene Blue from Aqueous Solution. *Polymers* **2021**, *13*, 4000. [CrossRef]
58. Abd El-Latif, M.M.; El-Kady, M.F.; Ibrahim, A.M.; Ossman, M. Alginate/Polyvinyl Alcohol -Kaolin Composite for Removal of Methylene Blue from Aqueous Solution in a Batch Stirred Tank Reactor. *J. Am. Sci.* **2010**, *6*, 280–292.
59. Al-asheh, S.; Banat, F. The Removal of Methylene Blue Dye from Aqueous Solutions Using Activated and Non-activated Bentonites. *Adsorpt. Sci. Technol.* **2003**, *21*, 451–462. [CrossRef]
60. El Miz, M.; Akichouh, H.; Salhi, S.; El Bachiri, A.; Tahani, A. Adsorption-desorption and kinetics studies of Methylene Blue Dye on Na-bentonite from Aqueous Solution. *IOSR J. Appl. Chem.* **2014**, *7*, 60–78. [CrossRef]
61. Ibrahim, S.; Ali, Z.T.A. Using of modified-bentonite as low-cost sorbent for removal of methylene blue dye from aqueous solution. *Assoc. Arab. Univ. J. Eng. Sci.* **2020**, *27*, 45–54. [CrossRef]
62. Ravi; Pandey, L.M. Enhanced adsorption capacity of designed bentonite and alginate beads for the effective removal of methylene blue. *Appl. Clay Sci.* **2019**, *169*, 102–111. [CrossRef]
63. Duwal, N. Investigation on the Selective Adsorption of Methylene Blue onto Clay Minerals of Kamerotarof Bhaktapur, Nepal. Master's Thesis, Tribhuvan University, Kathmandu, Nepal, 2013. [CrossRef]
64. Eleraky, M.I.; Abd, T.A.M.; Razek, E.; Elbasier, A.M.A. Removal of Methylene Blue Dye by Activated Egyptian Bentonite Clay. *J. Environ. Sci.* **2022**, *51*, 1–29. [CrossRef]
65. Taher, T.; Rohendi, D.; Mohadi, R.; Lesbani, A. Thermal and Acid Activation (TAA) of Bentonite as Adsorbent for Removal of Methylene Blue: A Kinetics and Thermodynamic Study. *Chiang Mai J. Sci.* **2018**, *45*, 1770–1781.
66. Benhouria, A.; Islam, A.; Boutahala, M.; Hameed, B.H. Calcium alginate–bentonite–activated carbon composite beads as highly effective adsorbent for methylene blue. *Chem. Eng. J.* **2015**, *270*, 621–630. [CrossRef]
67. Amrhar, O.; Nassali, H.; Elyoubi, M.S. Adsorption of a cationic dye, Methylene Blue, onto Moroccan Illitic Clay. *J. Mater. Environ. Sci.* **2015**, *6*, 3054–3065.
68. Chang, J.; Ma, J.; Ma, Q.; Zhang, D.; Qiao, N.; Hu, M.; Ma, H. Adsorption of methylene blue onto Fe_3O_4/activated montmorillonite nanocomposite. *Appl. Clay Sci.* **2016**, *119*, 132–140. [CrossRef]
69. Saratale, R.G.; Sun, Q.; Munagapati, V.S.; Saratale, G.D.; Park, J.; Kim, D.S. The use of eggshell membrane for the treatment of dye-containing wastewater: Batch, kinetics and reusability studies. *Chemosphere* **2021**, *281*, 130777. [CrossRef] [PubMed]
70. Sandollah, N.A.S.M.; Ghazali, S.A.I.S.M.; Wan Ibrahim, W.N.; Rusmin, R. Adsorption-desorption profile of methylene blue dye on raw and acid activated kaolinite. *Indones. J. Chem.* **2020**, *20*, 755–765. [CrossRef]
71. Auta, M.; Hameed, B.H. Modified mesoporous clay adsorbent for adsorption isotherm and kinetics of methylene blue. *Chem. Eng. J.* **2012**, *198–199*, 219–227. [CrossRef]
72. Banat, F.; Al-asheh, S.; Al-makhadmeh, L. Evaluation of the use of raw and acti v ated date pits as potential adsorbents for dye containing waters. *Process. Biochem.* **2003**, *39*, 193–202. [CrossRef]
73. De Castro, M.L.F.A.; Abad, M.L.B.; Sumalinog, D.A.G.; Abarca, R.R.M.; Paoprasert, P.; de Luna, M.D.G. Adsorption of Methylene Blue dye and Cu(II) ions on EDTA-modified bentonite: Isotherm, kinetic and thermodynamic studies. *Sustain. Environ. Res.* **2018**, *28*, 197–205. [CrossRef]
74. Azha, S.F.; Woon, L.K.; Ismail, S. Regeneration Feasibility of Bentonite by Sodium Persulfate. *Trends J. Sci. Res.* **2021**, *1*, 1–10. [CrossRef]
75. Taylor, P.; Unuabonah, E.I.; Adedapo, A.O.; Nnamdi, C.O.; Adewuyi, A.; Omorogie, M.O.; Adebowale, K.O.; Olu-owolabi, B.I.; Augustine, E.; Taubert, A. Desalination and Water Treatment Successful scale-up performance of a novel papaya-clay combo adsorbent: Up-flow adsorption of a basic dye. *Desalination Water Treat.* **2014**, *56*, 536–551. [CrossRef]
76. Shahadat, M. RSC Advances Regeneration performance of clay-based adsorbents for the removal of industrial dyes. *RSC Adv.* **2018**, *8*, 24571–24587. [CrossRef]
77. Sagita, C.P.; Nulandaya, L.; Kurniawan, Y.S. Efficient and Low-Cost Removal of Methylene Blue using Activated Natural Kaolinite Material. *J. Multidiscip. Appl. Nat. Sci.* **2021**, *1*, 69–77. [CrossRef]
78. Juzsakova, T.; Salman, A.D.; Abdullah, T.A.; Rasheed, R.T.; Zsirka, B.; Al-Shaikhly, R.R.; Sluser, B.; Cretescu, I. Removal of Methylene Blue from Aqueous Solution by Mixture of Reused Silica Gel Desiccant and Natural Sand or Eggshell Waste. *Materials* **2023**, *16*, 1618. [CrossRef] [PubMed]
79. Ghosh, D.; Bhattacharyya, K.G. Adsorption of methylene blue on kaolinite. *Appl. Clay Sci.* **2002**, *20*, 295–300. [CrossRef]
80. Al-futaisi, A.; Jamrah, A.; Al-hanai, R. Aspects of cationic dye molecule adsorption to palygorskite. *Desalination* **2007**, *214*, 327–342. [CrossRef]
81. Ngoh, Y.S.; Nawi, M.A. Role of bentonite adsorbent sub-layer in the photocatalytic-adsorptive removal of methylene blue by the immobilized TiO_2/bentonite system. *Int. J. Environ. Sci. Technol.* **2016**, *13*, 907–926. [CrossRef]